# SYNTHESIS OF SILVER-DIAMOND LIKE CARBON THIN FILMS

# BY MAGNETRON SPUTTERING

by

VENKATESH MAJJI

Presented to the Faculty of the Graduate School of

The University of Texas at Arlington in Partial Fulfillment

of the Requirements

for the Degree of

MASTER OF SCIENCE IN MATERIALS SCINCE AND ENGINEERING

THE UNIVERSITY OF TEXAS AT ARLINGTON

May 2013

ACKNOWLEDGEMENTS

I would like to express my heartful gratitude to my research advisor, Dr.Efstathios I. Meletis for his excellent guidance and constant encouragement throughout the research work. I am thankful to Dr. Tibbals and Dr. Liu for their participation as my defense committee members.

I am really thankful to Dr. Taktak for his help in my research work and moral support. I would also like to thank Jessica Mooney, Cristian Cionea, Adam J. Smith, Yishu Wang, Minghui Zhang, Elad Har-Even, Tapas Mehul Desai and Aida Mehdinezhad Roshan for their enduring help during the research work. I am thankful to the various UTA labs that helped in my research, Surface and Nano Engineering lab (SaNEL), Characterization Center for Materials and Biology.

I wouldn't have achieved this without the help of my beloved friends, Pradeep Badrachalam, Amir Salehi Gilani, Uday Kiran Gopalam, Kartik Machiraju, Anudeep Palanki and Gowtham Pedapudi for their encouragement and help. Finally, I like to express my sincere appreciation to my parents and family for their strong belief on me.

December 17, 2012

ABSTRACT

SYNTHESIS OF SILVER-DIAMOND LIKE CARBON THIN FILMS

BY MAGNETRON SPUTTERING

Venkatesh Majji, M.S.

The University of Texas at Arlington, 2013

Supervising Professor: Efsthathios I. Meletis

Diamond-like carbon thin films are been used in wide range of applications due to their attractive tribological properties. Metal-doped DLC films have significant properties which make them compatible to use in larger variety of applications. The present study examines the dispersion and their effect on various tribological properties when Ag is incorporated into the DLC thin films. These Ag-DLC nanocomposite films were synthesized by a hybrid CVD and magnetron sputtering process in a discharge composed of $CH_4$, and Ar atmosphere. These DLC and Ag-DLC films were characterized by Transmission Electron Microscopy (TEM), Fourier Transform Infrared Spectroscopy (FTIR), X-ray Photoelectron Spectroscopy (XPS) and Raman Spectroscopy. Tribological tests were carried out to measure the frictional and wear behavior of the Ag-DLC films as a function of Ag content.

The TEM cross sectional studies revealed that Ag is present as Ag nanoparticles that were distributed uniformly throughout an amorphous DLC matrix. XPS analysis confirmed that

Ag in the nanoparticles was present in the metallic form. Increasing the Ag content in the film, reduced its $sp^3$ content. The incorporation of these nanoparticles causes a reduction in hardness in Ag-DLC when compared with pure DLC films. Microhardness of DLC films exhibits values up to a maximum of 16 GPa and gradually decreases with increasing in Ag content. FTIR and Raman studies confirmed that the films contain a significant amount of hydrogen, and with an increase in the Ag content in the DLC film results in an increase in $sp^2$ carbon content. Finally, the friction behavior of the Ag-DLC films showed a comparable performance with that of DLC films with a coefficient of friction as low as 0.1. The DLC films exhibited a lower wear rate of $5.51 \times 10^{-8}$ $mm^3/Nm$ than Ag-DLC films. The wear rate in the Ag-DLC films gradually increased with increasing Ag content but it remained at low levels (i.e., up to $1.7 \times 10^{-7}$ $mm^3/Nm$). This is consistent with the higher $sp^2$ content of the Ag-DLC films.

TABLE OF CONTENTS

LIST OF ILLUSTRATIONS

Figure Page

LIST OF TABLES

# CHAPTER 1

## INTRODUCTION

Carbon can be available in different forms in the environment. One of its forms is diamond; it has a structure with a network of $sp^3$ domains and has proven to be a unique material with remarkable properties such as high hardness, optical transparency, thermal conductivity, chemical inertness, low wear rate with a limitation of high friction coefficient. The other is graphite; it has a structure with a network of $sp^2$ domains. Because of its layer like structure, it is a soft material having exceptional properties such as low friction coefficient, good electrical conductivity with a limitation of high wear rate. Diamond-like carbon (DLC), a new material obtained from both of these carbon forms and it consists of both $sp^3$ domains and $sp^2$ domains [1]. DLC is also referred to as amorphous carbon (a-C) or hydrogenated amorphous carbon (a-C:H) because of its short range property in structure. Diamond-like carbon had become one of the most attractive research areas after Aisenberg and Chabot's report in 1971 [2].

At low deposition temperatures, DLC thin films can be produced on different substrates with desirable properties like high hardness, thermal conductivity and good optical and electrical properties. It also has excellent biocompatibility, chemical inertness and tribological behavior, such as low friction rate and wear rate [3]. The latter makes it an attractive coating material on biomedical implants, wear resistant materials, antireflective materials and corrosion resistant material. Under some specific conditions, lubricating properties of both a-C and a-C:H films are well known. Due to formation of a graphite like transfer film in the sliding contact, the surface of these films are extremely smooth and the friction coefficient can be less than 0.1 or even as low as 0.01 depending on the nature of the coating and test conditions [4,5,6].

In this aspect, amorphous hydrogenated carbon DLC films have been extensively studied in the last two decades and have found a large number of applications [3] However, further

utilization is limited due to their low thermal stability (above 350°C), low toughness and adhesion [3,7]. It has been observed that above 400° C, graphitization of DLC film occurs by conversion of $sp^3$ carbon bonding to graphitic $sp^2$ bonding. Such temperatures can very well be reached during wear at asperity contacts and lead to 'wear induced graphitization' of DLC films, as proposed by Liu and Meletis. In other words, DLC films possess low toughness and these films are not thermally stable beyond $350^oC$, as they graphitize and exhibit low wear resistance [8].

Another drawback of DLC films is that they tend to delaminate or peel off when deposited above certain thickness. Due to presence of large inherent residual stresses the film has low adhesion and limited thickness [9]. In thin films, high compressive residual stresses originates from formation of $sp^3$ interatomic bonds and developed due to temperature changes, lattice mismatch, high energy of deposited ions and implantation of foreign atoms in the deposited films. Intrinsic stresses are developed during the growth of thin films. As the thickness of the films increase, the stresses increase causing the failure of the films by cracking, buckling and delamination even before the wear. Films with compressive stresses are more desirable than those with tensile stresses, as the former increases the strength whereas the latter causes cracks in the films. Stresses due to lattice mismatch can be avoided by using nitride and carbide interlayers. The other factor influencing the quality of films is the adhesive strength at the interface. For thin films, the stresses and the adhesion between the substrate and the film are interrelated. Improvement in the adhesion energy paves path for the prevention of buckling and delamination caused due to high stresses. Even the coefficient of friction of films decreases with the decrease in the stresses.

By the addition of metal atoms into the carbon matrix cause great changes in chemical and tribological properties of DLC coatings; such metal alloyed coatings are often denoted Me-DLC's. In Me-DLC composite films containing metal such as Cu or Ag inert with respect to carbon, interatomic forces in crystallite–carbon interfaces can be weak. These films may have

low internal stress, high ductility and toughness. In other words, the tribological behavior and friction properties of these Me-DLC composite films such as Cu-C or Ag-C films can be very distinct from those of carbide forming Me-DLC composite films [10]. There have been extensive studies on both Me-DLC coatings and conventional DLC coatings, which could be either hydrogenated or non-hydrogenated. Ag-DLC, has increasingly gained attention because of wide applications in optical device applications [11], cardiovascular devices or implants due to surface anti-bacterial properties [12], space devices because of wear resistance against oxygen plasma etching [13], for low-threshold field emitter application [14], for electrodes in electrochemical analysis in microelectromechanical systems [15] and tribological applications.

The present research focuses on fundamental aspects such as friction and wear tests that are reviewed firstly in this research work. Ag-DLC thin films were produced on to a $Si_{100}$ wafer and the tribological properties of these coatings were investigated using a pin-on-disk test geometry in dry sliding conditions. The friction coefficient is measured for different Me-DLC films at a constant loading condition and the results compared with each other. Chemical composition, surface morphology and microstructure of the worn wear tracks, debris and pin contact area were examined using complementary characterization techniques including Digital Microscopy, Optical Profilometry, Scanning Electron Microscopy (SEM), Energy Dispersive Spectroscopy (EDS), Transmission Electron Microscopy (TEM), X-ray Photoelectron Spectroscopy (XPS), FTIR and Raman spectroscopy.

# CHAPTER 2

## OBJECTIVE

The present research work involves diamond-like carbon to be doped by silver which is most beneficiary in biomedical applications. Hybrid Chemical Vapor Deposition/Physical Vapor Deposition (CVD/PVD) process is used to produce Ag-DLC thin films. Objectives of this work were to study:

- Effect of processing parameters on the characteristics of Ag-DLC films
- Structural properties of Ag- DLC films
- Frictional and wear behavior of Ag-DLC films

# CHAPTER 3

# LITERATURE REVIEW

## 3.1 Diamond–like Carbon Thin films

DLC films were fist deposited successfully by Aisenberg and Chabot by ionizing a carbonaceous source in an inert environment to form carbon ions onto a substrate and forming an amorphous layer of microcrystallites [2]. Deposition methods can be divided into two categories, namely Chemical Vapor Deposition and Physical Vapor Deposition. CVD involves decomposition of a carbon bearing gas phase on the substrate and the PVD methods use target materials such as graphite, carbon in the plasma deposition. Formation of DLC films is the result of bombardment of carbon or hydrocarbon radicals within a typical impact energy range of 100-1000 eV with the substrate [16]. Various methods are employed in synthesizing DLC films, prevalent methods include:

a. Ion beam deposition
b. Cathodic arc deposition
c. Laser ablation
d. Magnetron Sputtering
e. Plasma Enhanced Chemical Vapor Deposition

### *3.1.1 Fabrication Techniques for DLC synthesis*

#### 3.1.1.1 Ion Beam Deposition Methods

Ion beam deposition was the first method used for the synthesis of DLC. These methods use solid carbon targets or ionized hydrocarbon gases, ionization of hydrocarbon gases such as $CH_4$, $C_2H_6$, etc. yields carbon ions. In ionization, hydrogen is released by dissociation of molecules [17, 18]. In this method, an ion beam is formed from the plasma that is not in contact with the substrate and is directed at the substrate to bombard, thus resulting in

film growth. Since the ion energy can be controlled, a good process control is achieved. After the dissociation, hydrogen is deposited as a film in a high vacuum deposition chamber. The lower the pressure and power, the harder the films are. However, these conditions reduce the deposition rate.

Mass selected ion beam deposition is another method, where the deposition rate is controlled using monoenergetic ion species and low energy (<10 eV) carbon ions are produced from the graphite target [19]. The ions are accelerated through magnetic filter which blocks neutral ions. Electrostatic lenses are used to decelerate the ions to the required ion energies. Ion beam used under high vacuum conditions to prevent the possible damage during deposition [20]. The major advantage of this method is that it controls the deposition rate.

3.1.1.2. Filtered Cathodic Arc Deposition

The Filtered Cathodic Arc Deposition technique is optimal for producing hard tetrahedral amorphous carbon thin [21]. The device contains a magnetic filtering technique to remove effectively the macro particles and so enhances the smoothness of DLC film. Graphite acts as a cathode and chamber acts as an anode. When large arc currents in the range of 40-90 A are applied, carbon ions are produced between the cathode and anode. A bias voltage is applied at the substrate in the range of 100-300 V. It is used to regulate the ion energy in the chamber. The ta-C films produced have high $sp^3$ content in comparison to other techniques and exhibit greater hardness.

3.1.1.3. Magnetron Sputtering

Sputtering involves physical vapor deposition; high energy particles bombard the surface and eject atoms from the target material. High ion energy is needed to remove atoms from the target material resulting in good deposition. In magnetron sputtering, atoms emitted from target move towards the substrate, guided by magnetrons as there is lower impedance to their movement. During sputtering, high vacuum is maintained in order to keep ions at a high energy and to reduce collisions [22]. Plasma is produced by a voltage biasing with DC or RF

power. At appropriate gas pressure in the chamber and sufficient voltage across the electrodes, plasma discharge is developed. At the cathode, rapid ion acceleration along the sheath develops high electric dark sheath. Secondary electrons are released on colliding with cathode. Magnetrons are placed parallel to the cathode, creating a static magnetic field and based on Fleming's left hand rule, guides the emitted electrons in a direction perpendicular to both the applied electric field and the magnetic field. Near cathode, dense plasma is created when the gas atoms collide with the surrounded secondary electrons resulting in high deposition rates.

3.1.1.4. Pulsed Laser Deposition

Pulsed laser ablation is a deposition technique which produces hydrogen free diamond-like carbon films with high $sp^3$ content. Here, graphite or polycarbonate is used as target material and it is vaporized by using a pulsed excimer laser [19, 23]. As a result, dense plasma is generated and the vaporized target material gets deposited on to the substrate. The substrate can have a negative voltage bias or can be unbiased. The laser has intense energy, which can easily transform $sp^2$ domains to $sp^3$ domains, forming thin films that have a high hardness. The excimer laser's short wavelength property results in smooth surface of the deposited films.

3.1.1.5 Plasma Enhanced Chemical Vapor Deposition (PECVD)

In PECVD, generally hydrocarbon gases such as $CH_4$, $C_2H_2$, $C_2H_6$, etc. are used as precursor gases. Thus, the technique is very prominent for depositing hydrogenated amorphous carbon thin films. This technique produces good quality films at higher deposition rate and lower deposition temperature with least contamination [19, 24, 25, 26]. An appropriate Ar dilution ratio is selected and precursor gases are allowed to pass into deposition chamber. When a bias voltage is applied at the substrate at a low chamber pressure, it ionizes the hydrocarbon precursor producing plasma thereby attracting the ions required for growth of the film. The ion energy depends on the voltage applied and gas pressure which controls the $sp^3/sp^2$ ratio in hydrogenated amorphous carbon thin films. The working pressure, bias voltage and the hydrogen content considered as important parameters to obtaining quality films. The pressure

and bias voltage determine $sp^3$ /$sp^2$ ratio and deposition rate of the film whereas hydrogen minimizes the surface energy by passivating the dangling bonds resulting in low friction and helps in stabilizing the $sp^3$ bonds [19, 24, 25, 26, 27].

*3.1.2 Structure and Classification*

DLC films become a fascinating research area because of their structure, which makes DLC films a candidate material in wide applications such as automobile parts, magnetic storage disks, micro-electromechanical devices, reflective coatings for optical windows and biomedical applications for implantation [23, 28]. Its exceptional properties include low friction coefficient, high hardness, wear rate, thermal conductivity, electrical resistivity, chemical inertness, optical transparency and biocompatibility [25, 29].

Carbon exists in several allotropic forms, namely, diamond, graphite and polymer. It can form excessive range of crystalline and disordered structures as it can form in three stable hybridizations, $sp^3$, $sp^2$ and $sp^1$. Diamond has tetrahedral atomic structure with $sp^3$ hybridization, where strong sigma bond is formed between four valence electrons of carbon with their adjacent atoms. Graphite has trigonal shaped structure with $sp^2$ hybridization, where a strong sigma bond is formed between three of the four valence electrons and one weak π bond is formed with the remaining electron. Lastly, the $sp^1$ hybridization structure has two σ bonds and two π bonds. Hybridization of carbon schematic view is shown in Figure 3-1.

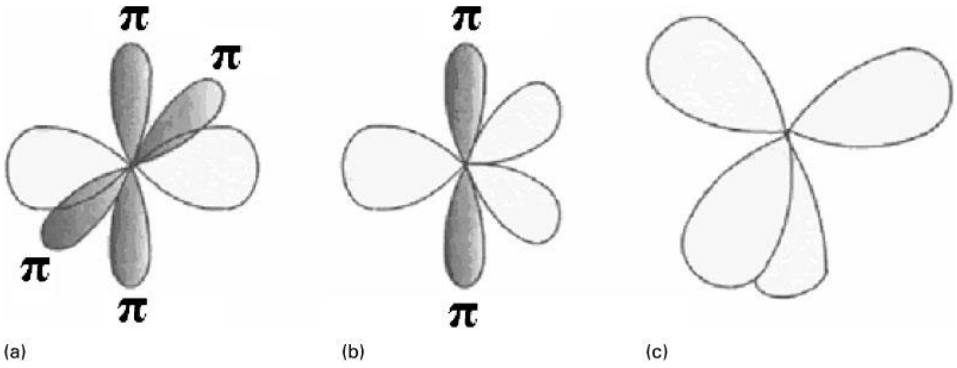


Figure 3-1 (a) $sp^1$ hybridization (b) $sp^2$ hybridization (c) $sp^3$ hybridization [19].

DLC films formed with a combination of diamond and graphite structure with some of the terminated hydrogen bonds. The diamond structure has 4-fold coordinated $sp^3$ sites, whereas the graphite structure has 3-fold coordinated $sp^2$ sites. Because of the presence of hybridization in short-range order, the films show amorphous. Films exhibit diamond-like properties if the $sp^3$ hybridization is dominant or graphite-like properties if $sp^2$ hybridization is dominant. Hydrogen content and doping material are the key factors, which determine the $sp^3$ and $sp^2$ content in the deposited film. Robertson has given a ternary phase diagram that shows the composition of DLC films in terms of $sp^3$ and $sp^2$ along with hydrogen content in Figure 3-2.

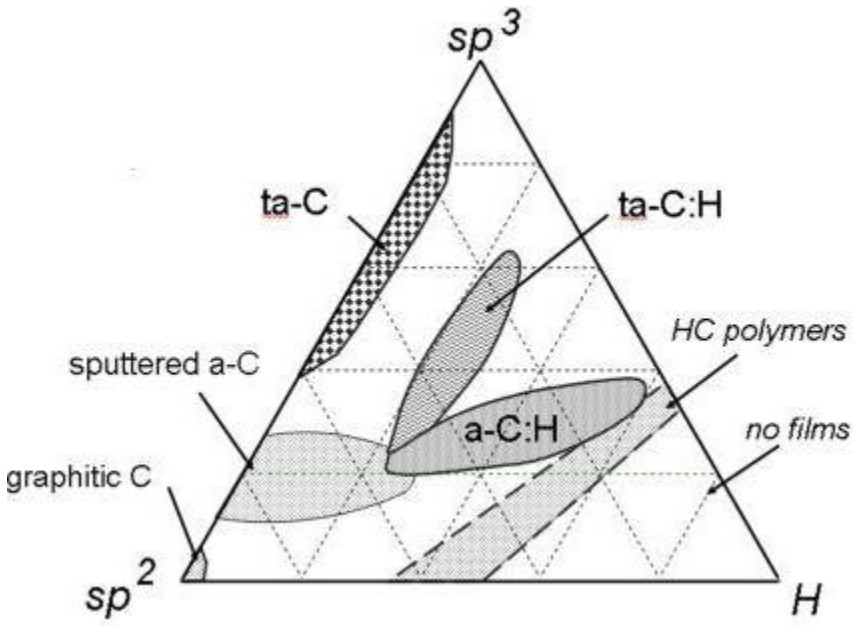


Figure 3-2 Ternary phase diagram of DLC [30].

DLC coatings are categorized into various groups with respect to change in the amount of hydrogen and $sp^3/sp^2$ ratio [31, 32, 33]. This phase diagram series begins with glassy structure and ends with tetrahedral amorphous carbon (ta-C) in considering $sp^3$ content. From Figure 3-2, it is evident that the materials in the bottom left corner have $sp^2$ hybridization with an amorphous carbon (a-C) structure. This group includes all the soft materials such as glassy carbon, soot, evaporated carbon and hars. Bottomed right corner consists of hydrocarbon

polymers, polyacetylene (CH)n and polyethylene ($CH_2$)n groups. Towards the top, formation of molecules is preferred over formation of long chains [19]. High amount of $sp^2$ bonds and low amount of $sp^3$ bonds combine to form a sputtered hydrogenated amorphous carbon (a-C:H) film. Very high amount of $sp^3$ bonded coatings are called tetrahedral amorphous carbon (ta-C). The central region of the phase diagram represents hydrogenated amorphous carbon (a-C:H), which contains higher amount of hydrogen and lower amount of $sp^3$ bonds. Near the top, tetrahedral amorphous hydrogenated carbon (ta-C:H) is formed, with a high amount of $sp^3$ bonds and low amount of hydrogen, All the various states of carbon properties are shown in the Table 3-1 [19]. Different techniques such as XPS, FTIR, and Raman Spectroscopy are used to characterize these coatings to determine the structural properties.

Table 3-1 Properties of various carbon forms [19].

| **Material** | **$sp^3$ %** | **Hardness (GPa)** | **H %** | **Density ($g/cm^3$)** | **Gap (eV)** |
|---|---|---|---|---|---|
| Diamond | 100 | 100 | -- | 3.5 | 55 |
| Graphite | 0 | - | -- | 2.267 | 0 |
| a-C ( evaporated) | 0 | 3 | -- | 1.9 | 0.4-0.7 |
| a-C (Sputtered) | 5 | 3 | -- | 2.2 | 0.5 |
| Ta-C | 80-88 | 80 | -- | 3.1 | 2.5 |
| a-C-H ( hard ) | 40 | 10-20 | 30-40 | 1.6-2.2 | 1.1-1.7 |
| a-C-H ( soft ) | 60 | < 10 | 40-50 | 1.2-1.6 | 1.7-4 |

## 3.2 Metal Doped-diamond-like Carbon Thin Films

There is huge research going on the DLC films because of their potential applications in automobile, biomedical and optical industries. Some of the limitations of DLC films are listed and discussed. First, the high compressive stress in the films developed during deposition, due to the formation of $sp^3$ bonds, resulting in poor adhesion. One of the theories is that these stresses are developed due to the film deposition at low substrate temperatures. Second limitation is the graphitization of DLC, Liu and Meletis [8] proposed the graphitization mechanism, stating that C-C bonds of $sp^3$ transform to $sp^2$ graphite when the temperature exceeds above 350°C, resulting in low coefficient of friction. A good method of avoiding these limitations is incorporating foreign atoms into DLC matrix.

### *3.2.1 Various metal doped DLC composite thin films*

The addition of metals such as Ti, WC, Ag, Cr, Cu, Nb, etc. to the DLC, lowers the internal stresses and these metals add a new phase thereby provide improved mechanical properties. Common method of synthesizing the metal doped films is physical vapor deposition which involves either sputtering of both graphite and doped material target or sputtering of the doped metal target in hydrocarbon environment using Ar as precursor gas. Corbella et al. [24] deposited metal doped DLC films by incorporating different metals such as Ti, Mo, W and Nb using PECVD technique. Kalges et al [34] states that low frictional properties were observed for metal-doped DLC films, proving the formation of carbide at lower level. The low frictional properties are attributed to the formation of transfer layer in both DLC and metal-doped DLC [35]. Experimental results prove that metals modify the DLC network; improving tribological properties such as wear rate and friction rate. Figure 3-3 shows the effect of metals change with respect to change in wear rate.

Co-DLC nanocomposite thin films were developed for the magnetic storage applications. These Co-DLC thin films were produced using hybrid CVD/PVD technique. The hardness tests performed on the cobalt based metal-doped film reveals a reduced hardness

from 11.3 GPa to 9 GPa when the cobalt content is increased from 50 at% to 65 at%, this is because of decrease in $sp^3/sp^2$ ratio from 1.3 to 0.87. But, friction rate of the films were increased with an incorporation of Co into DLC matrix [36]. Nanocomposite Cr-DLC films were produced with in the range of 0.1 at% to about 17 at% of Cr. It was found that, In Cr-DLC films, Cr is soluble in the DLC matrix if it is in the range of 0.4 and 1.5 at% but, Cr exists as defected Cr-carbide nanoparticles at higher Cr content. Results showed that, Cr-DLC films possess high hardness as well as they exhibit low friction rate (up to 12 at% Cr) and low stable wear rate about $10^{-7}$ $mm^3$/N-m [37].

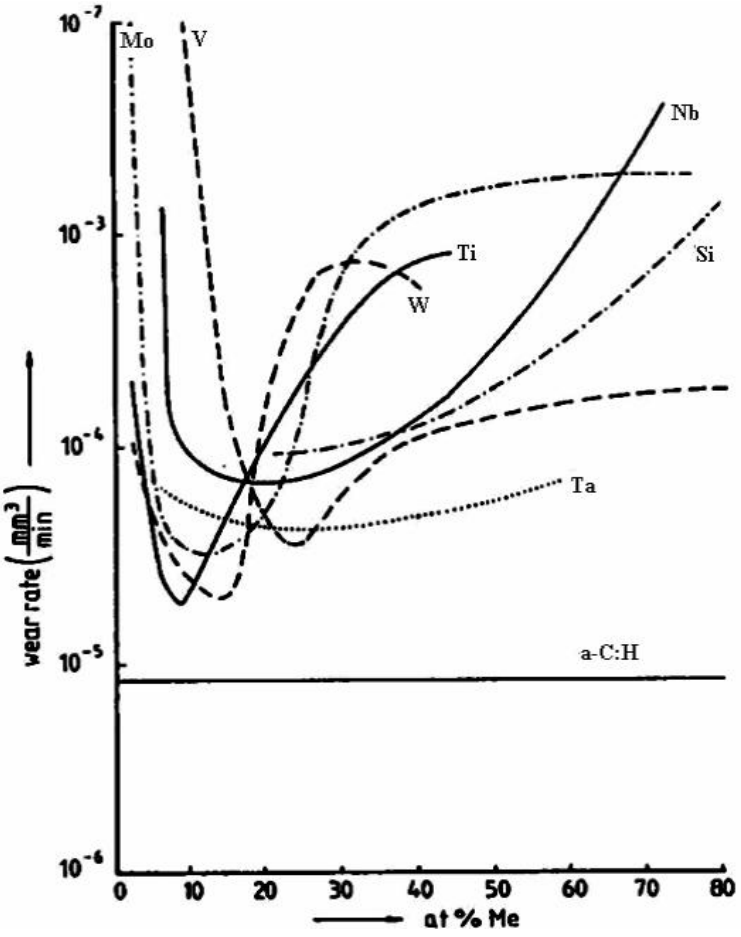


Figure 3-3 Wear rate of different Me-DLC's as a function of at.% Me [34]

*3.2.2 Ag doped DLC Thin Films*

While various Me-DLC like WC, Co, Cr Ti, Nb exhibit excellent tribological properties [24, 34, 35, 38], Ag incorporated DLC has numerous applications in biomedical and tribological industries [39, 40]. Zhang et al. deposited 5.5-5.6 at% silver-containing hydrogenated and hydrogen-free diamond-like carbon (DLC) nanocomposite thin films by plasma immersion ion implantation-deposition methods and compared friction and surface roughness properties of Ag/a-C:H and Ag/a-C thin films. The research done in Zhang et al. reported that Ag had more pronounced effect on a-C than a-C:H in terms of surface roughness and surface energy. Furthermore, Zhang et al. suggested that Ag content increases surface energy whereas hydrogen has an opposite effect. Therefore, a-C:H films have lower friction than a-C films, while Ag-DLC films had higher friction than pure DLC [41]. Lungu et al. incorporated C into the Ag film on bronze substrate at a concentration between 19 and 42 mass % by thermionic vacuum arc method. Lungu et al. found that C inclusion as DLC phase in the silver matrix reduced the coefficient of friction in dry sliding up to 2.5 times compared to that of the bronze substrate [42]. In another study, Lungu et al. reported that friction coefficient decreases when the grain size of film goes below 10 nm [40].

Narayan et al. deposited functionally gradient hydrogen-free Ag-DLC and Ti nanocomposites by using pulsed laser deposition on Ti-6Al-4V alloy. Narayan et al. reported that Ag-DLC films showed higher hardness (32 GPa) and E modulus (299 GPa) than Ti-DLC films (29 and 274 GPa). However, the coefficient of friction of Ag-DLC film (0.149) was higher than Ti-DLC (0.107) [43]. Xiang et al. deposited non-hydrogenated Ag-DLC films on silicon wafers, in a mid-frequency dual-magnetron system and they investigated influence of Ag content and grain size on microstructure and sliding tribological behaviors. Xiang et al. also found that the Ag nanocrystallites were dispersed in the DLC matrix, and increased Ag content will increase the grain size of Ag. The films with Ag content in between 3.3 and 11.4 at% having small grain sizes in the range of 5.4-16.8 nm exhibits high hardness, low intrinsic stress,

improved adhesion, and low friction coefficient and wear rate as compared with those of high gain size and content of the Ag. Xiang et al. suggested that the effective regime of Ag content for accomplishing low coefficient of friction, wear rate and good mechanical properties is in the range of 5 at% to 10 at% approximately. The best combined properties were achieved for the film deposited with 8.7 at% Ag and with grain size 12.9 nm [44]. Ag-DLC thin films were synthesized using hybrid CVD/PVD system, results shown that Ag nanoparticles of 4-7 nm in size were uniformly distributed in DLC matrix. Microhardness of DLC films exhibited a hardness of 22 GPa and it gradually decreases with increasing Ag content. As the Ag content increases, the $sp^3$ content decreases resulting in decreased film hardness [45]. Literature review shows that there is a little study on tribological properties of Ag-DLC. Zhang [41] compared Nano-frictional properties of hydrogenated and non-hydrogenated DLC thin films. The most detailed research for non-hydrogenated Ag-DLC in terms of tribological properties was carried out by Xiang [44]. However, the effect of the adding silver, which is used as a thin coating on hard substrates for tribological properties, is still unclear.

*3.2.3 Mechanical and Tribological Properties*

a. Hardness

In DLC films, the hardness is affected by the $sp^3$ content. The film with higher amount of $sp^3$ exhibits high hardness. Hardness and Young's modulus measurements are made with Nano-indenter. The maximum nano-hardness of hydrogenated amorphous carbon films and hard amorphous carbon films containing 85-90% $sp^3$ bonds are found to be 17 GPa, 80-88 GPa respectively [46]. Hardness is calculated from the given equation with respect to the yield stress and Young's modulus.

$$\frac{H}{Y} = 0.07 + 0.06\left(\frac{E}{Y}\right) \qquad [19]$$

Where H is the hardness, E is the young's modulus and Y is the yield stress.

b. Adhesion

Diamond like carbon thin films has applications in protective coatings because of their adhesive strength. However, these films have large internal compressive stresses preventing film growth, thereby making them useless [47, 48, 49]. It is assumed that the large internal stresses are developed during the subimplantation mechanism of DLC. This mechanism explains that large compressive stresses are developed when the incident energetic carbon species bombards an existing DLC and this is because during the deposition at room temperature, the atoms lack the mobility [47, 50]. If the internal stress exceeds a critical value, adhesive failure takes place and if the mechanical energy density exceeds the energy needed to create two new surfaces the thickness of the film, h, delaminates, such as

$$2G_1\left(\frac{1+\nu}{1-\nu}\right)hf^2 < 2\gamma$$

where, $\gamma$ is the surface/interfacial energy, $\nu$ is the Poisson's ratio, $G_1$ the shear modulus of the film and $f$ the strain in the film. There is research being done to improve the adhesiveness of the diamond like carbon thin films included depositing a metallic interlayers between the substrate and the DLC film, by incorporating foreign atoms and depositing carbide, forming adhesive layers [19, 51, 52, 53].

c. Friction coefficient

Frictional behavior depends on intrinsic and extrinsic factors such as degree of $sp^2$, $sp^3$ bonding and humidity [19, 33, 54]. DLC films are popular for their low frictional behavior because of $sp^2$ hybridization in their structure. The bonds broken in DLC during its formation, become passive due to the C-H bonds, rendering the film inert. Diamond surface is hydrophobic, closed shell bonded system and the contact between them is through the weak van der Walls forces. So, when the surfaces in contact shear, the weak van der Wall forces break resulting in deformation. At low humidity, when a-C:H comes in contact with the counter surface, a transfer layer of a-C:H is formed. The friction coefficient in this case is low as there is a contact between two hydrophobic a-C:H surfaces. Higher humidity causes transfer layer to

oxidize and thus hampers the formation of contact layer. Hence, in summary, there are no van der Walls forces in the DLC and the transfer layer is not hydrophobic, increasing the friction coefficient [19].

Lifang et al studied the frictional behaviors of DLC films against bearing steel balls and $Si_3N_4$ balls in different humid air and vacuum environments. The results show the variation of the friction coefficients of DLC films against the bearing steel balls and $Si_3N_4$ balls for the partially graphitized DLC films. The friction coefficient of DLC films against steel ball bearings in dry air is high; this is perhaps related with the oxidization of DLC films and its steel counterpart during sliding in dry air. The friction coefficient of DLC films against $Si_3N_4$ balls in vacuum is higher than in dry air due to the dehydrogenation and the graphitizing of the DLC film under the action of friction stress. Besides the hydrogen content of DLC films prepared in this study is only 26.7 at.%. This hydrogen content is lower than ordinal a-C:H films; this probably weakened the oxidization for DLC films during sliding in dry and humid air, thereby decreasing the friction coefficient [55].

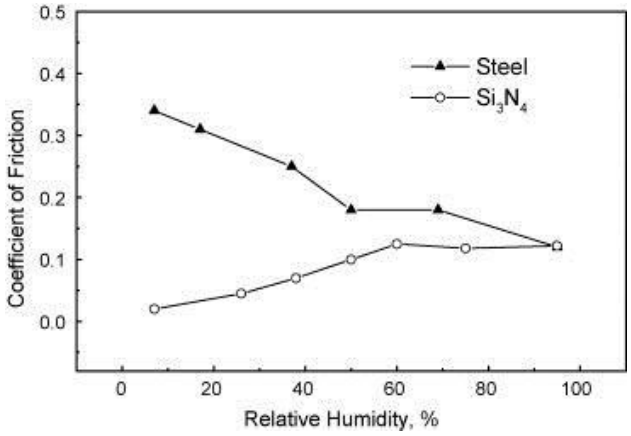


Figure 3-4 Friction coefficients of DLC films against bearing steel ball or $Si_3N_4$ ball vary with the increasing in the RH of air [55].

d. Wear

Wear depends on different factors like applied load, material's mechanical property and environmental conditions. The wear rates for DLC films are as low as $10^{-8}$ $mm^3$/Nm. Addition of metals or other elements such as silicon into the films can lead to further reduction in wear rate [56]. Baba et al. deposited Ag-DLC films by Magnetron Plasma Source Ion Implantation. He reported that tribological properties of DLC films are affected when they doped with Ag. He also states that the surface roughness is increased with silver content in the films and best wear properties were derived for the DLC films with 1.8 at. %Ag. [57]. Wei et al conducted wear tests and compared wear rates between pure DLC, Cu-DLC and Ti-DLC. They used a "crater grinding method" based on microabrasion mechanism to do wear tests of the films under a constant load of 5g. Figure 3-5 shows the wear test results for the DLC, Cu-DLC and Ti-DLC films on silicon. They observed that the effect of titanium is stronger than that of copper. One possible explanation for this behavior is that titanium forms strong carbide bonds in the film, compared to Cu [58].

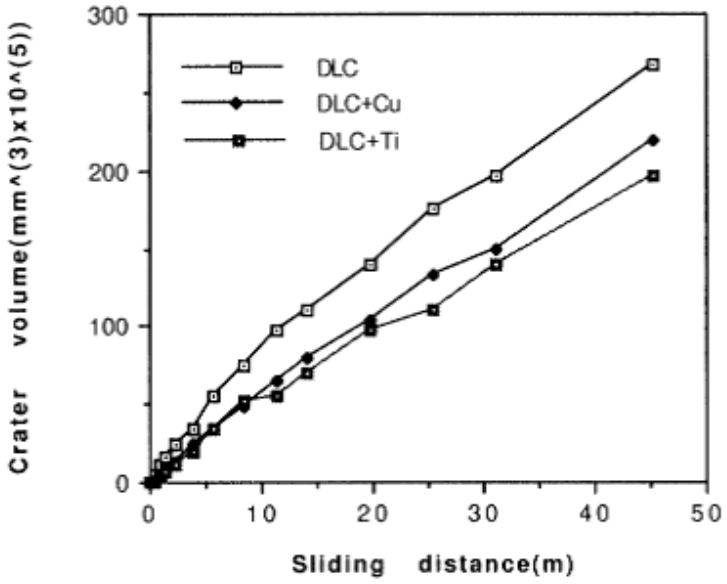


Figure 3-5 Wear test results of pure DLC, Cu-DLC and Ti-DLC [58].

*3.2.4 Applications of DLC Thin films*

a. Automobile Industry

DLC coatings have been used in automotive industry for the past few decades. The coatings have become a solution for manufacturing tools or systems used in the industry, providing reduced maintenance, improving efficiency, extending tool life and boosting the performance without having any effect from the substrate properties. Automotive industry demands Low friction rate with high wear resistance for good lubricant performance and the DLC coatings provide a solution for these automobile applications in manufacturing components such as gears, valve filters, fuel injector parts and wrist pins. The DLC coatings also enhance properties such as hardness and wear resistance making them applicable in manufacturing cutting and abrasive wear instruments such as drills and manufacturing machines.

b. Biomedical Industry

DLC films also can also be used biological applications, for components implanted into the human body. These coatings have also been applied for the orthopedic implants like blood pumps, heart valves and load bearing joints. Functionally graded multilayer DLC films prepared by pulsed plasma techniques of DLC are being studied for their medical applications [43]. Figure 3-6 shows (a) hip joint and (b) an artificial hip joint [59].

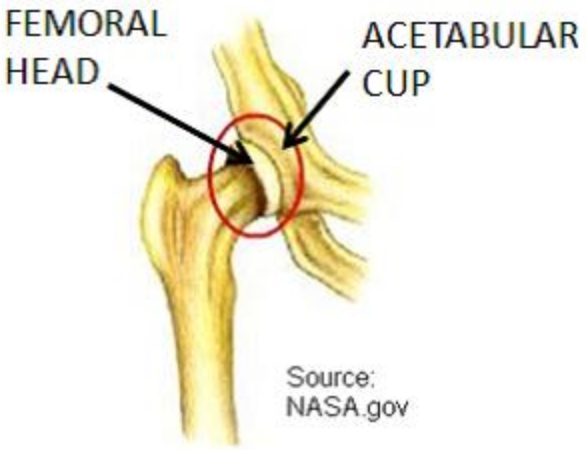


(a)

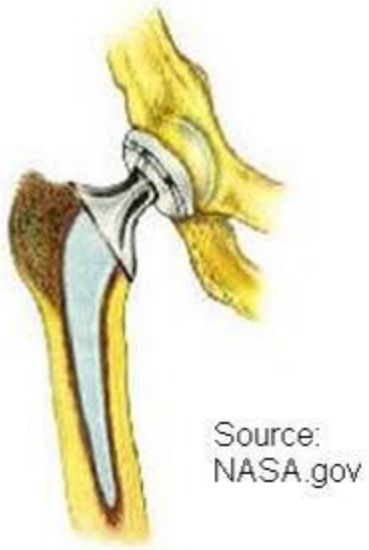


(b)

Figure 3-6 (a) Hip Joint, (b) Artificial hip joint [59].

c. Magnetic storage devices

The best achievement of these DLC thin films is improved magnetoresistance in high recording media; the storage density has improved up to 200 Gb/inch$^2$ for longitudinal recording

applications. The ultra-thin DLC films also improved wear and corrosion protection of magnetic hard disks. Because of its ultra-thin, atomically smooth, and dense properties, the gap between recording head and the disk minimized resulting in achieving large storage densities [60]. Me-doped DLC thin films for metals such as Co, Fe are used in recording media applications [61]. Co-DLC composites are mostly deposited on recording heads at the head-disc interface to improve corrosion resistance and mechanical wear [62]. The devices like magnetic and microwave circuits, magnetic recording media and magneto optical recording are being coated with magnetic thin films.

d. Optical devices

DLC films have been used in optical storage devices due to their improved transparence, band gap, and improved hardness. DLC films also have other optical applications such as decorative coatings, phase-shift masks and electroluminescence and this has its applications in controls interfacial colors. Current research is focused on solar photovoltaic applications due to the semiconducting nature of the Films [63]. Synthesizing the DLC structures are proven to be cheaper than silicon based cells. In the research field, regulating defects and doping of diamond-like carbon structures are issues being addressed. Pure DLC and Nitrogen doped DLC are being coated as antireflective coatings on silicon solar cells improving their refractive index and reducing the adsorption coefficient.

# CHAPTER 4

# EXPERIMANTAL PROCEDURE

This chapter provides a brief description on how the process parameters, bias voltage, DC current and chamber pressure affects the deposited film properties. In recent years, for depositing nanolayered/multi layered thin films, different deposition techniques are in use for large/small scale industries such as Ion beam deposition, Sputtering, Cathodic arc, Laser ablation, Plasma enhanced CVD, etc. In our present research, for effective investigation and for accurate results, all the experiments are carried out on a home-built hybrid Plasma enhanced Chemical Vapor Deposition (i.e. Magnetron Sputtering) system. Construction and main components of the system were explained later in this section. Both DLC and Metal doped DLC's were successfully deposited through this process using methane and Argon as precursor gases. Finally, a study on silver content in diamond-like carbon on mechanical and tribological properties of the films was performed.

## 4.1 Processing System: PECVD/PVD

### *4.1.1 Plasma enhanced CVD/PVD*

The DLC films have been synthesized by a home-built PECVD/PVD system. Figure 4-1 shows a schematic representation of its design and components. The cylindrical shaped stainless steel chamber is 18.38'' in diameter and 19.66'' in length. This chamber has the substrate holder, three magnetron guns and various different gauges installed into the system. It is connected to a cryopump to achieve very clean vacuum. The substrate has both RF and DC biasing connections, and it also has rotation for uniform deposition over the sample. It can be heated for up to 850° C and a thermocouple is attached to measure the substrate temperature. The temperature can be easily changed during the deposition process according to the requirements. The 4" endplate substrate holder can hold a maximum of 4" diameter samples.

The three magnetron guns placed on the floor of the chamber can hold thicknesses of 0.125", 0.185" and 0.250" targets. Magnetrons aid to direct ions coming from the target after its bombardment towards the substrate, and applied magnetic field prevents diversion of these ions according to Fleming's left hand rule. Pneumatic shutters are used as a shield over the magnetron guns. The gun can be DC biased for up to 1 kW through an MDX 10 K DC power supply and RF biased through an RF generator. Either bias type causes plasma production within the chamber when applied between the substrate and the floor of the chamber.

Roughing is achieved by a mechanical rotary valve pump. It depressurizes the lines, the cryo pump, and the deposition chamber to 25 mtorr. A cryo compressor helps to cool the arrays within the cryopump to 10 K. Next, base pressure of ~$3x10^{-6}$ torr was achieved in the deposition chamber by a cryo pump. As mentioned in the beginning, three different pressure gages are installed, first gauge is thermocouple gauge and it measures the roughing line pressure. Second one is a Baratron gauge, it measures chamber pressure during deposition and provides input to the cryopump gate valve for maintaining a set point pressure during deposition. Last is the ion gauge, which measures the pressure when the chamber is exposed to the high vacuum cryo pump. The ion gauge operates only under a pressure below $10^{-4}$ mtorr. The precursor gases are controlled through mass flow controllers and a read out box during deposition.

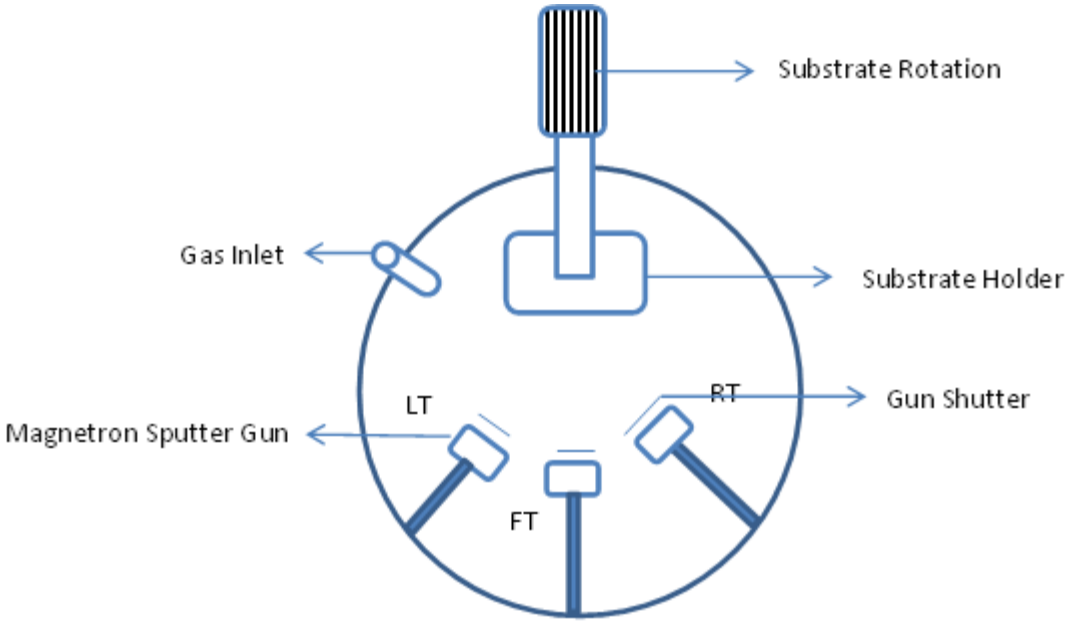


Figure 4-1 Schematic representation of hybrid PVD/CVD system.

*4.1.2 Deposition Procedure for DLC and Ag-DLC thin films*

All the DLC and Ag-DLC films were deposited on 2" Si (100) p-type wafers by the above mentioned hybrid PECVD technique. The wafers were first ultrasonically cleaned in acetone and then blown dry with compressed air prior to loading into the chamber. The wafer was masked in two regions at the edges, which were later used to determine the film thickness using step height analysis. The chamber was roughed down to 20mtorr using the mechanical pump and then exposed to the cryopump by opening the gate valve. The base pressure of the chamber was around $1x10^{-6}$ mtorr.

Prior to deposition, the chamber was purged two times with Argon. The substrate was sputtered, cleaned with Argon at a bias of -1000 V for 5 min at 50 mtorr. Sputter cleaning allows good adhesion of the deposited films by eliminating any surface contamination present through energetic argon ion bombardment. Then the system was again evacuated to high vacuum. After sputter cleaning, thin films were deposited by negative biasing of the substrate in a discharge

composed of $CH_4$, Ar atmosphere. The CH4/Ar ratio was adjusted by controlling their individual flow rate and the chamber pressure was adjusted to the required level.

While continuously cooling the substrate with water, it was biased at -500 V, rotation set to 20 rpm. After the pressure and flow rates were stabilized, DC voltage was applied to the substrate and plasma is generated. The films were allowed to deposit at 60 min, 120 min and 180 min in majority of the cases. After deposition, the sample was cooled inside the chamber in the presence of argon. Thus a series of Ag-DLC thin films were deposited by varying the parameters like $Ar/CH_4$ ratio, working pressure, DC current as shown in Table 4-1.

Table 4-1 DLC and Ag-DLC Experimental conditions.

| Sample | DC Bias to Substrate (V) | WP (mTorr) | CH4/Ar Ratio | DC Power to Target (mA) | Deposition Time (min) |
|---|---|---|---|---|---|
| Ag-DLC 1 | -1000 | 40 | 30/70 | 20 | 60 |
| Ag-DLC 2 | -500 | 40 | 30/70 | 20 | 60 |
| Ag-DLC 3 | -1000 | 40 | 20/80 | 20 | 60 |
| Ag-DLC 4 | -1000 | 40 | 20/80 | 20-40 | 60 |
| Ag-DLC 5 | -1000 | 40 | 15/85 | 20-40 | 60 |
| Ag-DLC 6 | -1000 | 40 | 10/90 | 20-40 | 60 |
| Ag-DLC 7 | -1000 | 40 | 15/85 | 60 | 60 |
| Ag-DLC 8 | -1000 | 40 | 10/90 | 60 | 60 |
| Ag-DLC 9 | -1000 | 40 | 15/85 | 100 | 60 |
| Ag-DLC 10 | -1000 | 40 | 10/90 | 100 | 60 |
| Ag-DLC 11 | -1000 | 40 | 20/80 | 60 | 60 |
| Ag-DLC 12 | -1000 | 40 | 15/85 | 70 | 60 |

Table 4-1 - *Continued*

| | | | | | |
|---|---|---|---|---|---|
| Ag-DLC 13 | -1000 | 40 | 15/85 | 60 | 60 |
| Ag-DLC 15 | -1000 | 40 | 15/85 | 20 | 60 |
| Ag-DLC 16 | -1000 | 40 | 15/85 | 40 | 60 |
| Ag-DLC 17 | -1000 | 40 | 15/85 | 65 | 60 |
| Ag-DLC 18 | -1000 | 40 | 15/85 | 50 | 60 |
| Ag-DLC 19 | -1000 | 40 | 15/85 | 70 | 60 |
| Ag-DLC 20 | -1000 | 40 | 15/85 | 60 | 60 |
| Ag-DLC 21 | -500 | 40 | 15/85 | 60 | 60 |
| Ag-DLC 22* | -1000 | 40 | 15/85 | 40 | 180 |
| Ag-DLC 23 | -1000 | 40 | 15/85 | 60 | 180 |
| Ag-DLC 24* | -1000 | 40 | 15/85 | 70 | 180 |
| Ag-DLC 25* | -1000 | 40 | 15/85 | 80 | 180 |
| Ag-DLC 26* | -1000 | 40 | 15/85 | 100 | 180 |
| Ag-DLC 27 | -1000 | 40 | 15/85 | 90 | 180 |
| Ag-DLC 28* | -1000 | 40 | 15/85 | 120 | 180 |
| Ag-DLC 29 | -1000 | 40 | 15/85 | 70 | 180 |
| Ag-DLC 30* | -1000 | 40 | 15/85 | 60 | 180 |
| Ag-DLC 31 | -1000 | 40 | 10/90 | 60 | 120 |
| Ag-DLC 32 | -1000 | 10 | 15/85 | 40 | 60 |
| Ag-DLC 33 | -1000 | 20 | 15/85 | 100 | 60 |
| Ag-DLC 34* | -1000 | 20 | 15/85 | 100 | 60 |
| Ag-DLC 35* | -1000 | 30 | 10/90 | 100 | 60 |
| DLC 1 | -1000 | 40 | 15/85 | - | 120 |
| DLC 2* | -1000 | 30 | 15/85 | - | 120 |

## 4.2 Characterization of DLC and Ag-DLC Thin films

### *4.2.1 Thickness, Roughness and Deposition rate*

The masked areas of the Si wafers reflect the film thickness. Both the thickness of the film and surface roughness were measured by a WYKO NT 1000 surface optical profilometer which functions on the principle of light interference at a magnification of 10X. The surface profiler was operated under PSI mode and captured surface data, 3-D interactive display and x, y profiles for thickness and roughness for all the samples. Both film thickness and surface roughness values signify the average of at least three measurements. Film thickness and deposition time determines the deposition rate.

### *4.2.2 Structural Characterization Techniques*

#### 4.2.2.1 Scanning Electron Microscopy (SEM)

The cross section morphology of the deposited films and the compositional analysis of the Ag-DLC films were characterized by Scanning Electron Microscopy in conjunction with Energy Dispersive Spectroscopy (EDS). Samples were characterized at an acceleration Voltage of 20 keV.

#### 4.2.2.2 Fourier Transform Infrared (FTIR) Spectroscopy

FTIR spectroscopy was conducted to obtain C-H bonding characteristics and determine $sp^3/sp^2$ ratios in the deposited film. A Nicolet FTIR system operated in transmission mode was used for the analysis of the samples. The absorption response of the films is obtained by subtracting the spectrum of DLC and Ag-DLC films from the Si wafer background. The resultant curve was smoothed twice using 25 point smoothing in the OMNIC software. The resulting spectrum of deposited films was deconvoluted in the regions of interest using Origin 8.0 software. Curve fitting was performed on the deconvoluted peaks in a Gaussian distribution and the area under the component peaks was noted for $sp^3/sp^2$ ratio determination.

4.2.2.3 Transmission Electron Microscopy

High-resolution transmission electron microscopy (HRTEM) of Ag-DLC samples were performed on Hitachi H-9500 HRTEM electron microscope operated at 300 keV with a point-to-point resolution of 0.18 nm. Cross sectional slices were obtained by cutting the samples along a direction normal to the coating surface and then gluing, face to face, the two coating surfaces. Cross-sectional specimens for TEM observation were prepared by mechanical polishing, and dimpling followed by Ar-ion milling using a Gatan Precision Ion Polishing System (PIPSTM, Model 691) with double mode at an angle of $4^{o}$. Examinations were conducted to determine the distribution of Ag nanoparticles in the DLC matrix. The structural characterization was conducted by selected area electron diffraction pattern analysis.

4.2.2.4 Raman Spectroscopy

Raman spectra provides abundant information regarding the amorphous films structure due to its ability to distinguish between $sp^3$ and $sp^2$ bonding types. Raman measurements were obtained using a laser of wavelength 532 nm with a low input power of 2.5 mW in order to minimize possible beam-heating effects. All bands in the Raman spectra have been fitted using a Gaussian line shape.

4.2.2.5 X-Ray Photoelectron Spectroscopy

The binding energy of C atoms in the DLC and Ag-DLC films was determined using XPS. XPS surface analysis was performed with Perkin-Elmer spectrometer using Al Kα monochromatic x-ray source (1484.6 ev). The principle involves X-ray bombardment on to the sample and the kinetic energy of photo-excited core electrons is determined from the samples as a measure of their binding energy. The pressure was maintained below $10^{-9}$ Torr. The survey spectra were obtained at constant pass energy of 100 eV taken in increments of 0.5 eV with dwell times of 100 ms for 5 scans. The high resolution spectrum of each element was obtained at 50 eV pass energy taken in increments of 0.2 eV with dwell times of 100 ms for at least 200 scans. To investigate the chemical state of the C-atoms, high resolution peak spectra was

obtained. Using CASA software, the peaks were deconvoluted, the amount of $sp^2$and $sp^3$ in deposited thin films was determined based on their areas.

*4.2.3 Characterization of Mechanical and Tribological Properties*

4.2.3.1 Nanoindentation

The hardness, *H*, and indentation modulus, $E/(1-V^2)$, were measure using a Hysitron Ubi 1 nanonindenter. Nanoindentations on the DLC and various Ag-DLC thin films of thicknesses above 250 nm were carried out on a three-sided, Berkovich-type pyramidal indenter. The indenter shape function was obtained by an assumption of indenter contact depth independent modulus, using a fused silica as the calibration specimen. The force was different on each film, but the force was chosen in order to maintain an indentation depth just below 10% of the coating thickness.

4.2.3.2 Pin-on-disc Experiments

Pin-on-disc tests were performed on DLC and Ag-DLC films to illustrate their tribological behavior i.e. wear rate and friction coefficient of the deposited film. The pin material is a 440C steel ball of 9.5mm diameter for the experiments. A constant load of 5N was applied for these experiments. These wear tests were performed in the presence of laboratory air with a relative humidity of 40 ± 10%, at a 10 cm/s sliding velocity over a distance of 1000 m. The friction coefficient was monitored continuously as a function of sliding distance.

By observing the wear track profile under a stylus profilometer, the wear rate was obtained. The wear volume was measured by multiplying the cross sectional area of the wear track with the length of the wear track. The wear rate of the film is given by:

$$Wear\ rate = \frac{\text{Wear Volume } (mm^3)}{Load\ (N) X\ Sliding\ Distance\ (m)}$$

SEM observations were performed on the wear tracks and also on the pin scar to determine possible transfer layer formation. Optical microscopy was used to find the diameter of the wear

scar. The wear volume in the ball was calculated by measuring the diameter of the wear scar and using the below formula:

$$Wp = \frac{\pi D^4}{64\, r}$$

Where, *Wp* is pin wear volume, *D* is average diameter of the scar and *r* is pin radius.

CHAPTER 5

RESULTS AND DISCUSSION

## 5.1 Characterization

### *5.1.1 TEM*

The samples namely, Ag-DLC 22 (2 at.%) and Ag-DLC 26 (8.3 at.%) were selected for characterization by TEM analysis. Both samples deposited at a negative biasing of 1000 V at different DC powers connected to the target of 40 mA, and 100 mA, respectively. The films deposited at 40 mTorr pressure in a mixture of inert gas (85 sccm of Ar) and carbonaceous gas (15 sccm of $CH_4$). TEM Analysis involves the cross sectional view of the deposited film using high resolution transmission electron microscopy. Figure 5-1 shows cross sectional view of the film consisting of the silicon substrate, the substrate/film interface and the Ag-DLC film. Elemental analysis of C, Ag was performed at different llocations of the film in the direction to its growth. Figure 5-1 shows 6 different locations of the elemental analysis and Table 5-1 presents the content of Ag at each location.

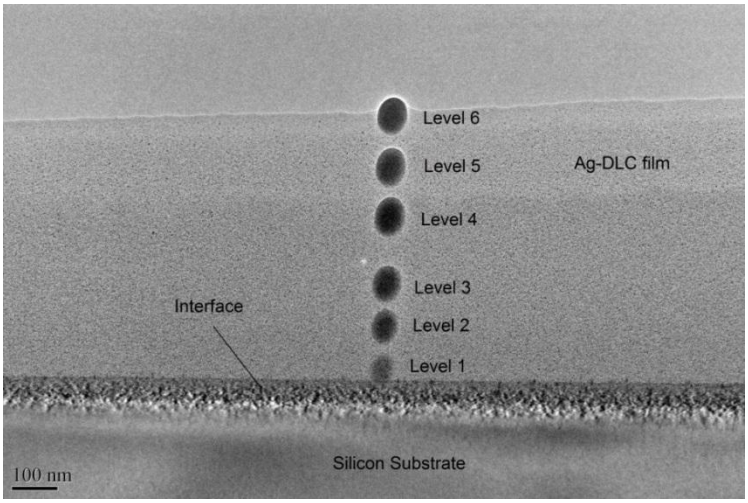


Figure 5-1 Elemental analysis of Ag content at different stages of the film for Ag-DLC (2 at.%).

Table 5-1 Ag content at different locations of the film Ag-DLC (2 at%).

| Level | Atomic % Ag |
|---|---|
| 1 | 10.9 |
| 2 | 9.8 |
| 3 | 7.7 |
| 4 | 3.6 |
| 5 | 0.6 |
| 6 | 0.1 |

It was observed that the silver content decreases form the interface to the top of the film surface as the film grows having an average of 2 at.%. It was showing, higher amount of silver deposited in the beginning at level 1 (near the interface) i.e., 10.9 at.% Ag, later it decreased to 9.8at.% Ag at level 2, finally it reached 0.1 at.% Ag at level 6 as the growth of the film increases. But total deposition rate remained constant. This suggests that poisoning of the target is occurring as the deposition progresses. Due to carbon accumulation on to the top of the target, the silver atoms can't get ejected from target surface resulting in less silver deposition. Figure 5-2 shows that there is uniform distribution of silver within the network of DLC with an interatomic distance of about 2-5 nm, stated that the silver particles are encapsulated by the DLC network. There was also formation of agglomerated silver particles near the interface giving an appearance of a needle like structure. The dark spots represent Ag nanoparticles whereas the bright regions represent the network of diamond-like carbon as is clearly shown in Figure 5-4.

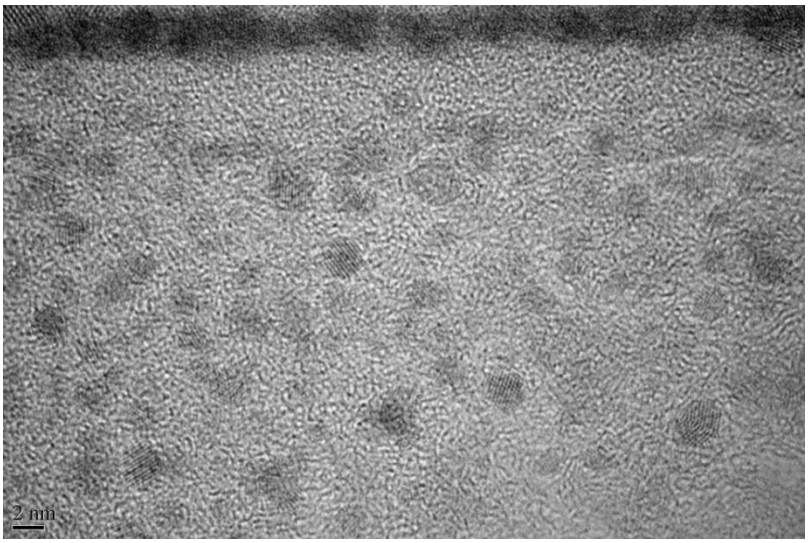


Figure 5-2 Ag dispertion in DLC matrix for Ag-DLC (8.3 at.%Ag).

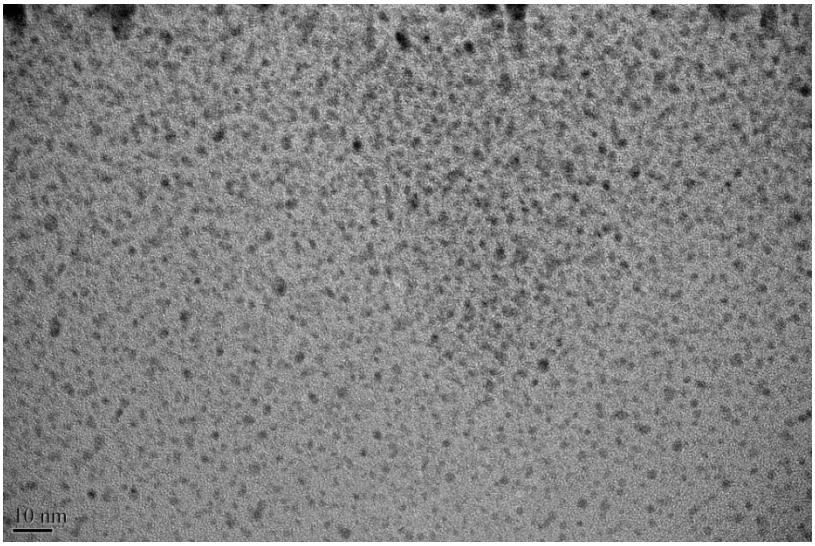


Figure 5-3 Ag dispertion in DLC matrix for Ag-DLC (2 at.%Ag).

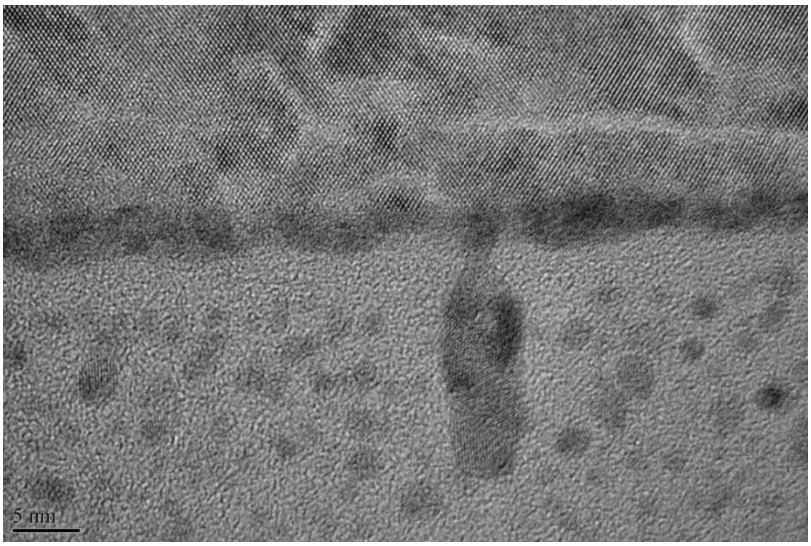


Figure 5-4 Needle –like structure of agglomerated particles of Ag near the interface.

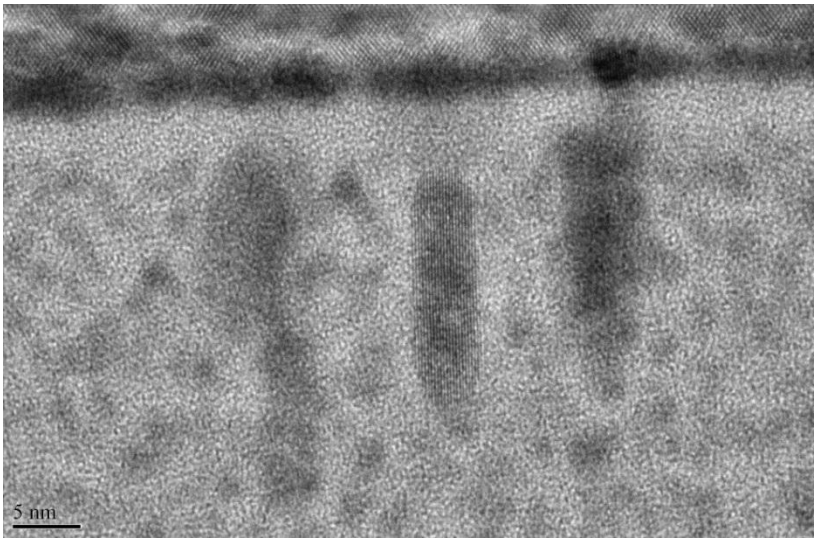


Figure 5-5 High resolution of film substrate interface.

5.1.2 XPS

X-Ray Photoelectron Spectroscopy was used to investigate the binding energy of C atoms in the DLC and Ag-DLC films. X-rays are irradiated on the sample and the kinetic energy

of photo-excited core electrons is determined as a measure of their binding energy. This method is useful for analysis up to a depth of 10 nm. XPS spectra were obtained by using a Perkin Elmer digital 500 instrument. The source was Al-K$\alpha$ (1486.6 eV) excited to 300 watts, the spot size was 2x3 mm and the pass energy was 8.95 eV.

Figures 5-6, 5-7 and 5-8 show high resolution XPS spectra of DLC and Ag doped DLC samples. These figures clearly indicate that the spectra consist of C 1s (~284 eV) and O 1s (~532 eV) peaks for DLC film and there is a contribution of Ag 3d (~368 and 374 eV) peaks as well as peaks of C 1s and O 1s for Ag containing DLC. The oxygen peak at about 532 eV was probably due to contamination formed at the surface of the samples with air exposure. Since XPS is a very surface sensitive technique, the detection of oxygen suggests various sources of surface contamination [17].

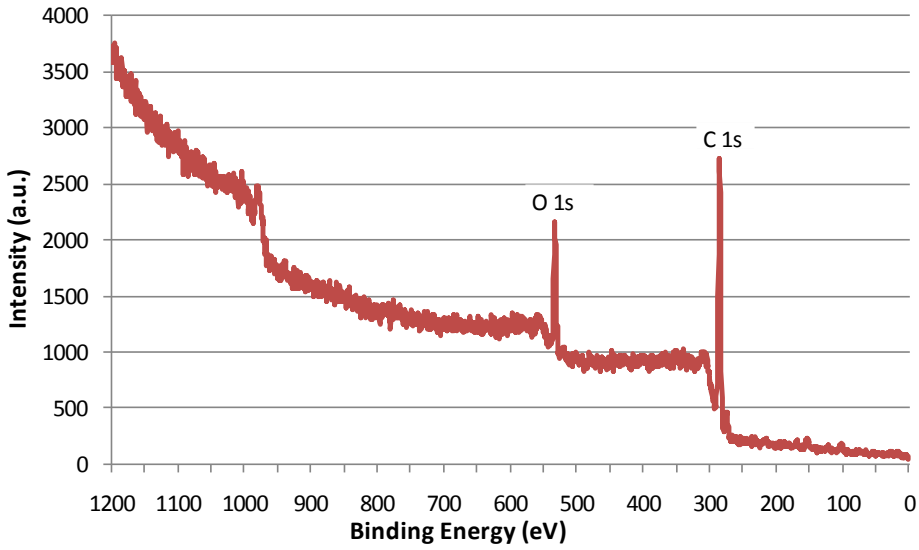


Figure 5-6 XPS survey spectrum from DLC thin film.

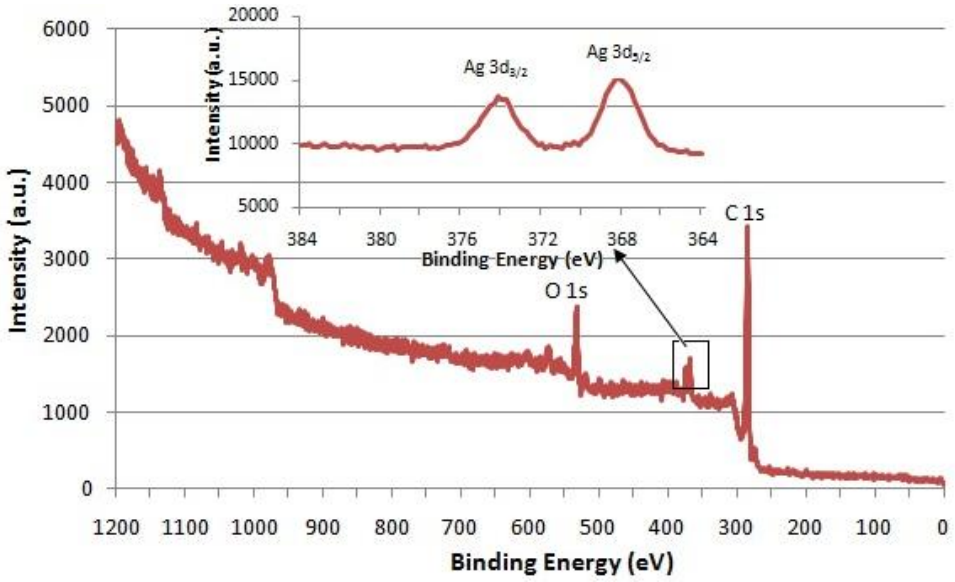


Figure 5-7 XPS survey spectrum from DLC thin film containing 3 at % Ag.

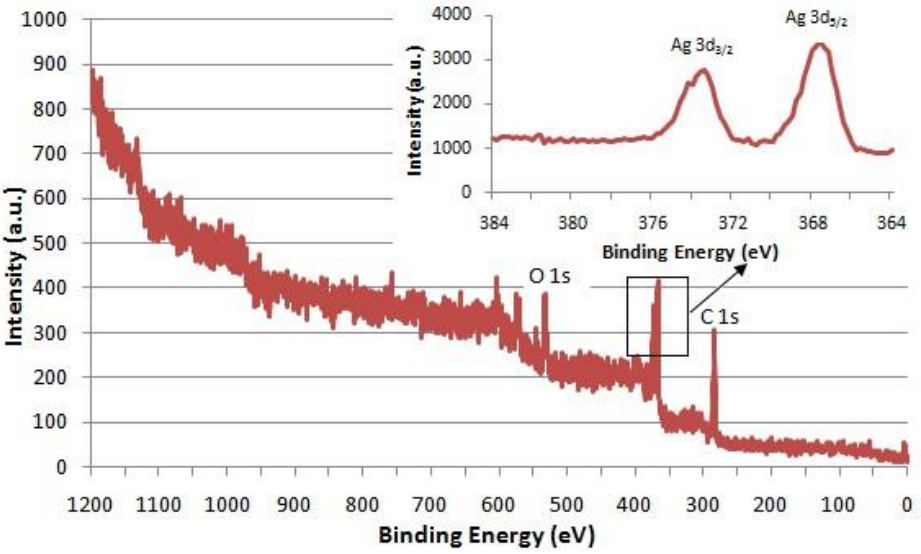


Figure 5-8 XPS survey spectrum from DLC thin film containing 8.3 at % Ag.

As seen in Figures 5-6, 5-7 and 5-8, the Ag 3d region consists of two binding energy peaks corresponding to Ag $3d_{5/2}$ at 368.2 eV and $3d_{3/2}$ at 374.2 eV, respectively, which suggests

that the silver has been incorporated into the DLC matrix. The Ag ions can be inferred to exist in the metallic state, that is, without forming bonds with the matrix C atoms. Figure 5-9, 5-10 and 5-11 presents high resolution C 1s peaks for DLC and 3 and 8.3 at % Ag containing DCL films, respectively. Percentage of $sp^2$ and $sp^3$ in C 1s spectra of DLC and Ag-DLC thin films is given in Table 5-2. The C 1s peak can be deconvoluted into two components with binding energies at 284.4-284.5 eV and at 284.8-285 eV corresponding to $sp^2$ C-C and/or C-H (olefin/graphite) and $sp^3$ C-C and/or C-H (CH3), respectively [18].

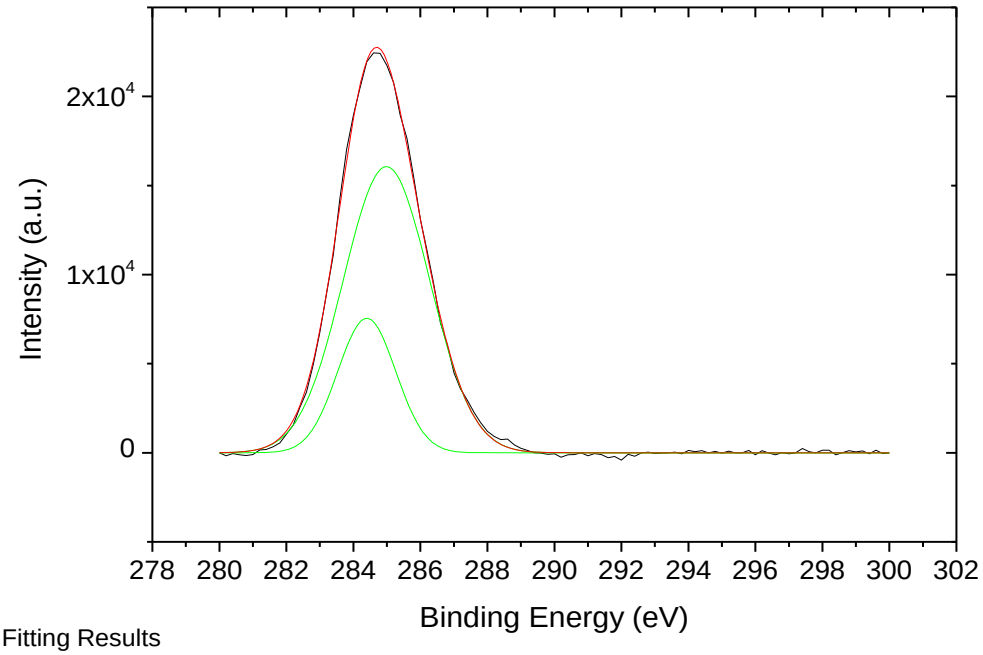


Fitting Results

| Peak Index | Peak Type | Area Intg | FWHM | Max Height | Center Grvty | Area IntgP |
|---|---|---|---|---|---|---|
| 1. | Gaussian | 16363.43068 | 2.03788 | 7543.33263 | 284.40137 | 24.04118 |
| 2. | Gaussian | 51700.75261 | 3.02498 | 16057.0183 | 284.98799 | 75.95882 |

Figure 5-9 Deconvolution of high resolution of C 1s peak of DLC film.

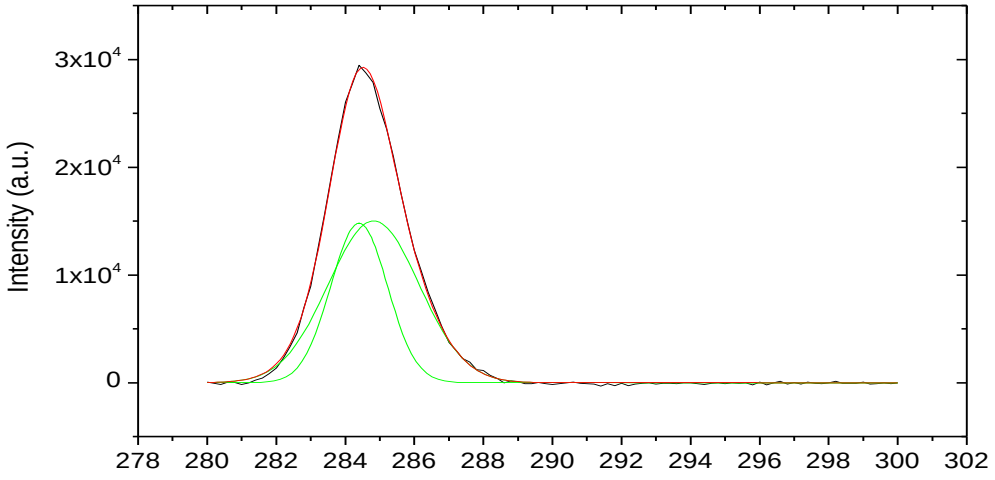


Fitting Results

| Peak Index | Peak Type | Area Intg | FWHM | Max Height | Center Grvty | Area IntgP |
|---|---|---|---|---|---|---|
| 1. | Gaussian | 30500.53014 | 1.93622 | 14798.58867 | 284.4 | 38.03019 |
| 2. | Gaussian | 49700.30517 | 3.11097 | 15010.27463 | 284.82282 | 61.96981 |

Figure 5-10 Deconvolution of high resolution of C 1s peak of DLC thin film containing 3 at % Ag.

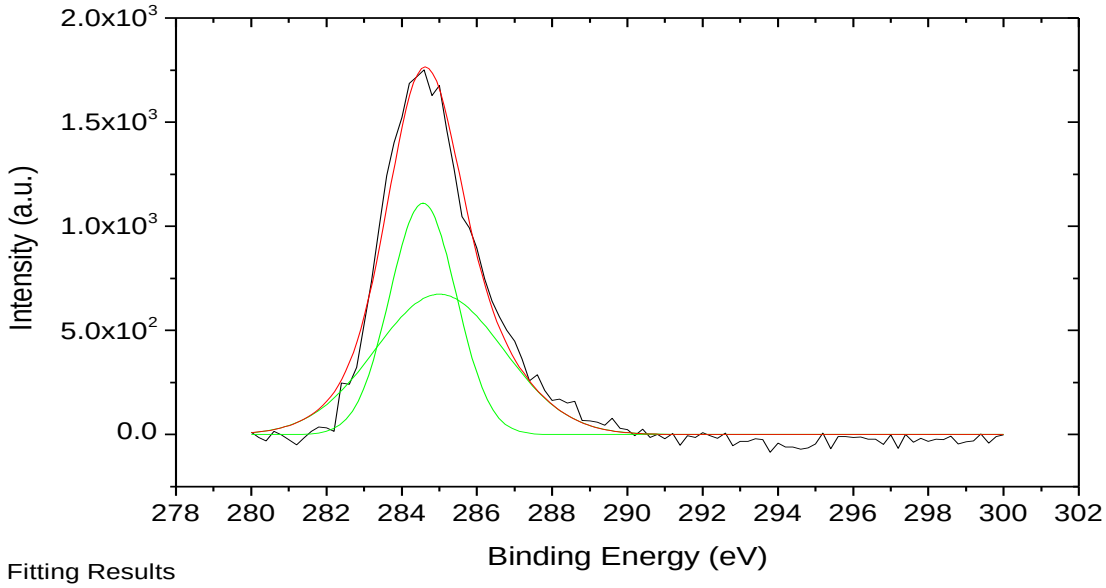


Fitting Results

| Peak Index | Peak Type | Area Intg | FWHM | Max Height | Center Grvty | Area IntgP |
|---|---|---|---|---|---|---|
| 1. | Gaussian | 2448.3181 | 2.0715 | 1110.32748 | 284.56768 | 45.99684 |
| 2. | Gaussian | 2874.47827 | 4.01328 | 673.98833 | 285.00354 | 54.00316 |

Figure 5-11 Deconvolution of high resolution of C 1s peak of DLC thin film containing 8.3 at % Ag.

Table 5-2 Percentage of $sp^2$ and $sp^3$ in C 1s spectra of DLC and Ag-DLC thin films.

| Sample | Binding Energy (eV) | | Peak contribution (%) | |
|---|---|---|---|---|
| | $sp^2$ | $sp^3$ | $sp^2$ | $sp^3$ |
| DLC | 284.4 | 284.98 | 24 | 76 |
| Ag-DLC (3 at %) | 284.4 | 284.82 | 38 | 62 |
| Ag-DLC (8.3 at %) | 284.56 | 285 | 46 | 54 |

The $sp^2$ ratio increases with increasing Ag content in the DLC. The film structure significantly changes with increasing atomic percentage of silver, which is most evident from the increasing intensity of the $sp^2$ and the decreasing intensity of the $sp^3$. It is thus evident that the DLC film changes to more graphitic as the Ag concentration increases [19]. These results are in agreement with the previous experimental observations (FTIR and Raman) in the present study.

### 5.1.3 FTIR

FTIR spectra were taken for all samples to investigate the C-H bonding in the films. Strong FTIR absorption of the C-H stretch was obtained in the range 2800-3150 $cm^{-1}$ which reveals a high H content in the films. A Nicolet FTIR system was used for the analysis. The spectrum of DLC and Ag-DLC films was subtracted from the Si wafer background to obtain the absorbance response of the films. The resultant curve was smoothed twice using 25 point smoothing in the OMNIC software. The region for C-H stretching was selected and was subjected to a base line correction. The corrected curve was subjected to Fourier Self Deconvolution to get the component peaks. The deconvoluted peaks were curve fitted in a Gaussian distribution and the area under the component peaks was noted for their percentage determination.

Figure 5-12 shows FTIR spectra from obtained from the DLC and Ag-DLC thin films. Generally, the vibration mode of the FTIR spectrum obtained from a-C:H films is classified into stretching-type and deformation-type bands. The vibration mode of the stretching-type carbon-hydrogen bond is observed in the range of 2850-3305 $cm^{-1}$ and that of the deformation-type is observed in the range of 1300-1700 $cm^{-1}$. In our examination, only the stretching-type vibration mode was observed for the DLC films.

The C-H stretching mode is revealed at 2800-3300 $cm^{-1}$ of the FTIR absorption spectrum. The $CH_3$ asymmetric stretching vibration occurs at around 2975-2950 $cm^{-1}$, whereas for the absorption occurs at about 2930 $cm^{-1}$. The $CH_3$ symmetric vibration occurs at about 2865-2885 $cm^{-1}$ and the $CH_2$ absorption occurs at about 2870-2840 $cm^{-1}$. As seen in Figure 5-12, after wave number of 2950 $cm^{-1}$ with increasing of Ag content into DLC, absorption peaks shifted up. This implies that hydrogen content of the thin films changed accordingly $sp^3/sp^2$ ratio changed.

Deconvoluted FTIR spectra of C-H stretch for DLC and Ag-DLC are shown in Figure 5-13 and the various bonding states of the C-H stretching and also role of Ag in the DLC films are given in Table 5-3. The relative amount of each bonding type was obtained by estimating the area under each peak. As seen in Fig 5-13 – Figure 5-18, with introducing of Ag into DLC, the shoulders at ~2800-2850 $cm^{-1}$ and at ~2970-3150 $cm^{-1}$ arising due to $sp^3$-CH symmetric and $sp^2$-CH olefinic stretching vibrations became prominent, respectively. The obvious absorption peaks at 2830-2920 and 2960-2980 $cm^{-1}$ are due to the hydrogen atom in the $CH_2$ (sym-asym) / $CH_3$ (sym) stretching bands, all bonded to $sp^3$-type carbon. The peaks located at 2950 $cm^{-1}$ and in the range of 3000-3110 $cm^{-1}$ may be assigned to $sp^2$-$CH_2$ (sym) and $sp^2$-CH (olef./arom.) bonding stretching modes. From these results, it can be said that the bonding structures between carbon and hydrogen in DLC and Ag-DLC films consists of $sp^3$ and $sp^2$ bonds.

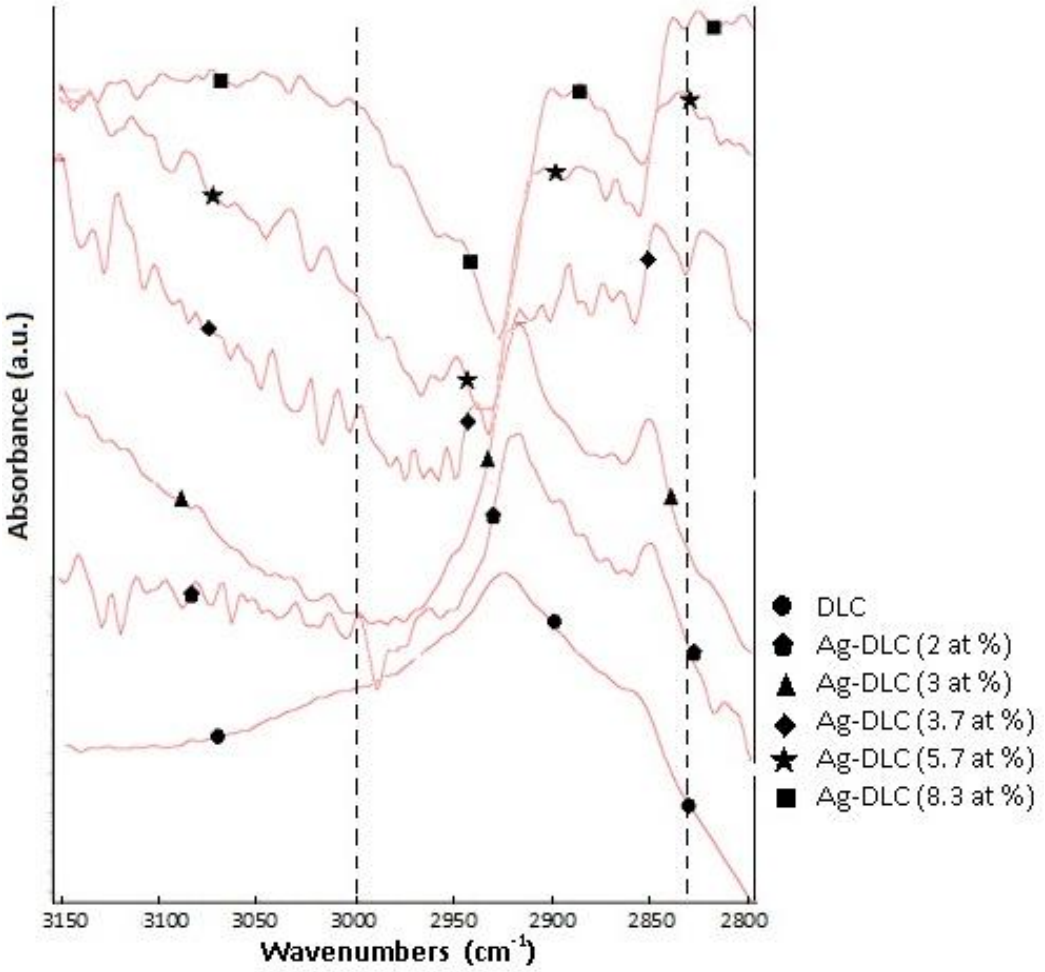


Figure 5-12 Comparison of FTIR spectra obtained from the DLC and Ag-DLC thin films.

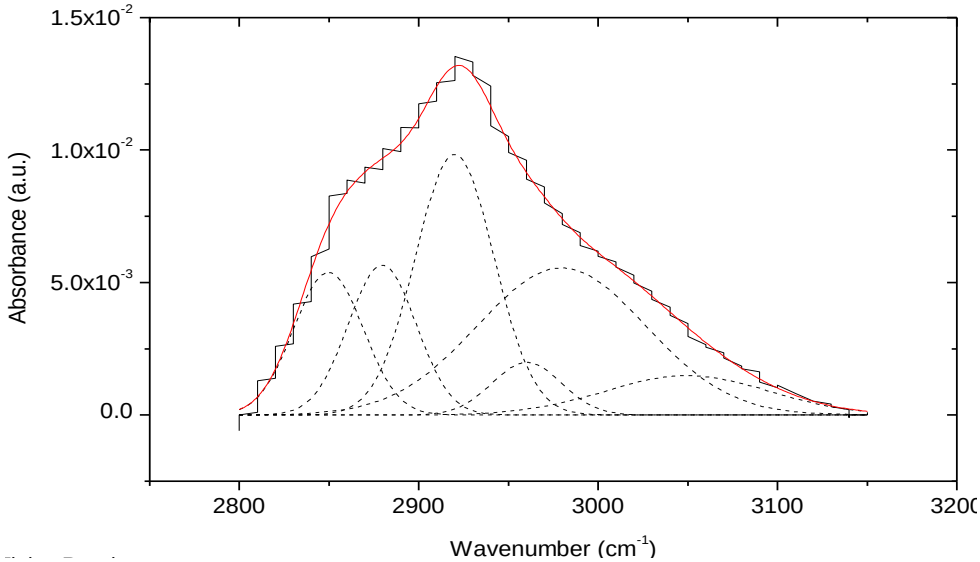


Figure 5-13 Deconvolution of the C-H stretch for DLC thin film.

Table 5-3 FTIR vibrational mode assignment in the C-H stretch region for DLC film.

| DLC $sp^3/(sp^2+sp^3)$ ratio : 91.6 % | | |
|---|---|---|
| **Wavenumber, $cm^{-1}$** | **Assignment** | **Peak contribution, %** |
| 2850 | $sp^3$ $CH_2$ (sym) | 13.1 |
| 2880 | $sp^3$ $CH_3$(sym) | 13.5 |
| 2920 | $sp^3$ $CH_2$(sym) | 27.3 |
| 2960 | $sp^3$ $CH_3$(asym) | 4.8 |
| 2980 | $sp^3$ $CH_2$(asym) | 32.9 |
| 3050 | $sp^2$ CH (arom.) | 8.4 |

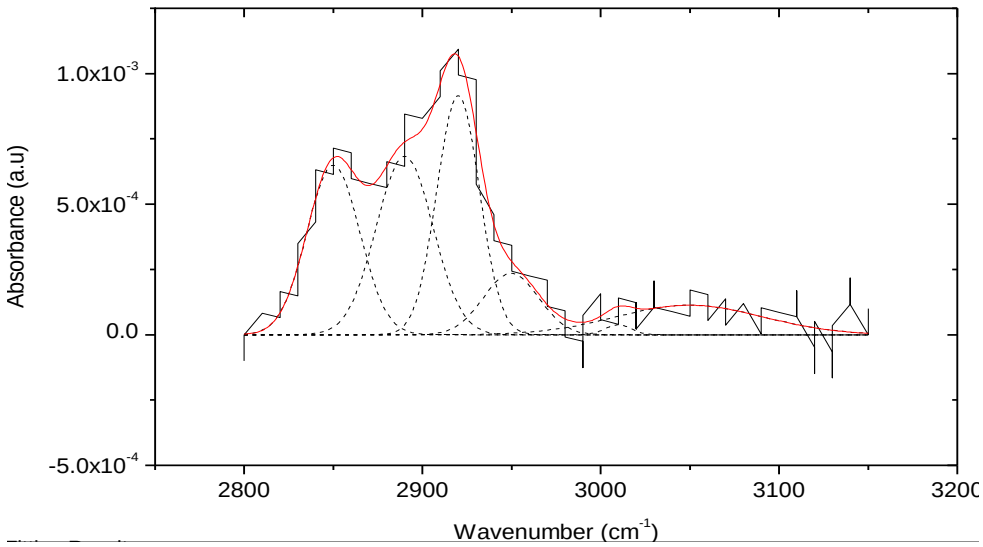


Figure 5-14 Deconvolution of the C-H stretch for Ag-DLC film containing 2 at % Ag.

Table 5-4 FTIR vibrational mode assignment in the C-H stretch region for Ag-DLC film containing 2 at% Ag.

| Ag-DLC17 (2 at %) $sp^3/(sp^2+sp^3)$ ratio : 82.6 % | | |
|---|---|---|
| **Wavenumber, $cm^{-1}$** | **Assignment** | **Peak contribution, %** |
| 2850 | $sp^3$ $CH_2$(sym) | 26.1 |
| 2890 | $sp^3$ $CH_2$(sym) | 29.2 |
| 2920 | $sp^3$ $CH_2$(sym) | 27.3 |
| 2950 | $sp^2$ $CH_2$ (sym) | 5.1 |
| 3010 | $sp^2$ CH (olef.) | 0.7 |
| 3050 | $sp^2$ CH (arom.) | 11.6 |

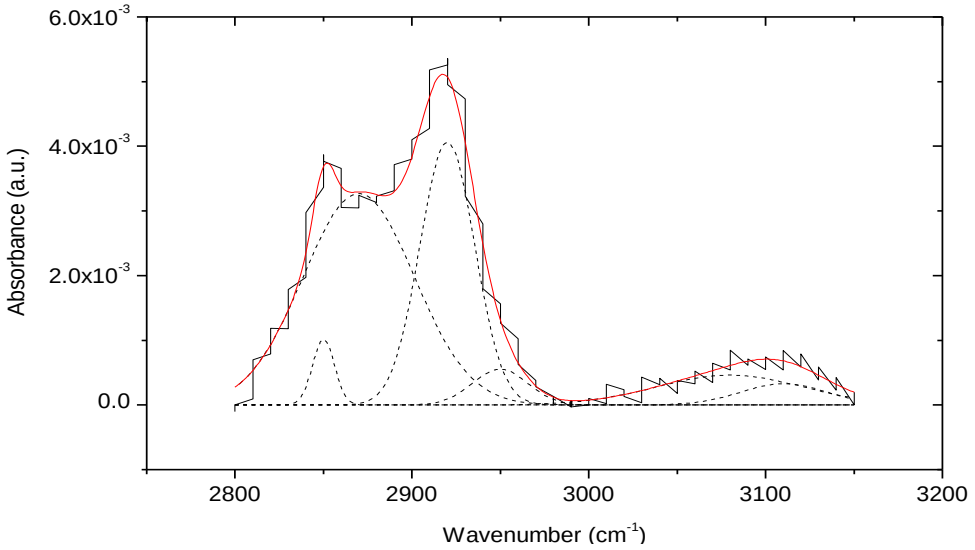


Figure 5-15 Deconvolution of the C-H stretch for Ag-DLC film containing 3 at % Ag.

Table 5-5 FTIR vibrational mode assignment in the C-H stretch region for Ag-DLC film containing 3 at% Ag.

| Ag-DLC33 (3 at %) $sp^3/(sp^2+sp^3)$ ratio : 80.2 % | | |
|---|---|---|
| **Wavenumber, $cm^{-1}$** | **Assignment** | **Peak contribution, %** |
| 2850 | $sp^3$ $CH_2$(sym) | 3.1 |
| 2870 | $sp^3$ $CH_3$(sym) | 48.4 |
| 2920 | $sp^3$ $CH_2$(sym) | 28.7 |
| 2950 | $sp^2$ $CH_2$ (sym) | 7.2 |
| 3080 | $sp^2$ CH (olefinic) | 8.9 |
| 3110 | $sp^2$ CH (olefinic) | 3.7 |

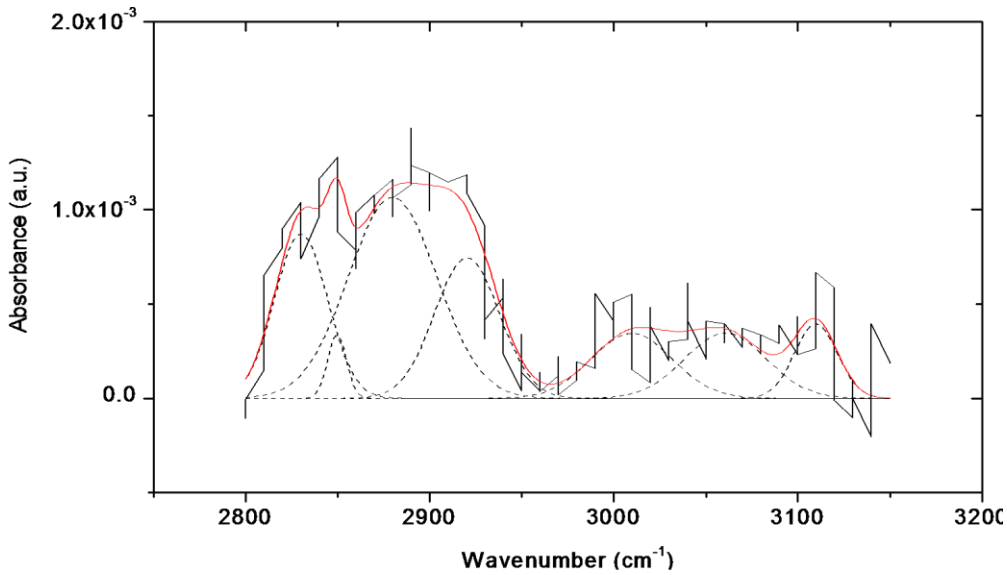


Figure 5-16 Deconvolution of the C-H stretch for Ag-DLC film containing 3.7 at % Ag.

Table 5-6 FTIR vibrational mode assignment in the C-H stretch region for Ag-DLC film containing 3.7at%Ag.

| Ag-DLC27 (3.7 at %) $sp^3/(sp^2+sp^3)$ ratio : 79.4 % | | |
|---|---|---|
| **Wavenumber, $cm^{-1}$** | **Assignment** | **Peak contribution, %** |
| 2830 | $sp^3$ $CH_2$(sym) | 21.3 |
| 2850 | $sp^3$ $CH_2$(sym) | 1.7 |
| 2880 | $sp^3$ $CH_2$(sym) | 41.2 |
| 2920 | $sp^3$ $CH_2$(sym) | 15.2 |
| 3010 | $sp^2$ CH (olefinic) | 17.8 |
| 3110 | $sp^2$ CH (olefinic) | 2.8 |

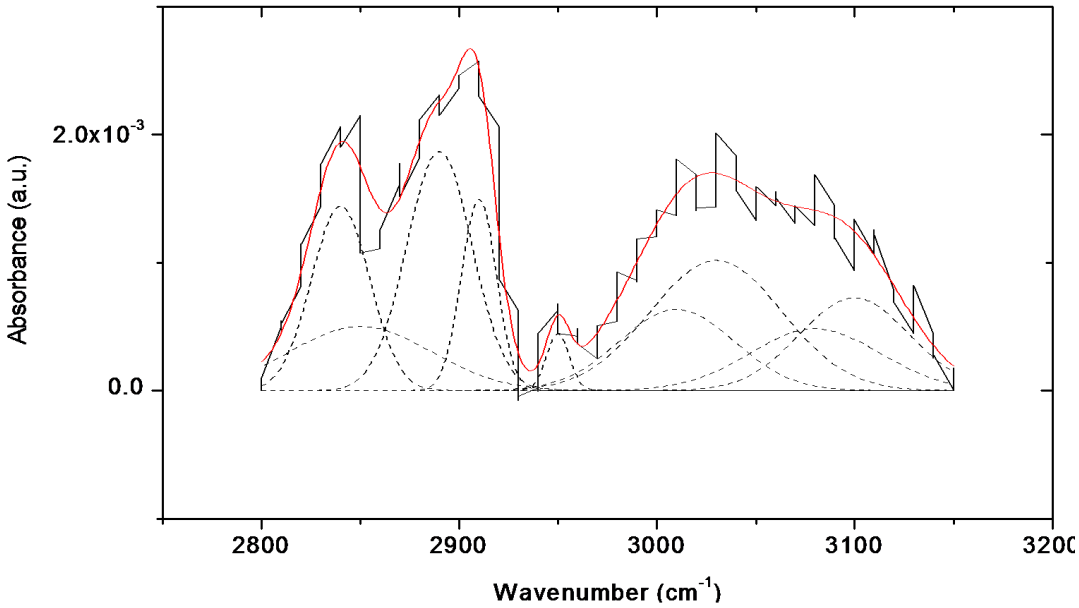


Figure 5-17 Deconvolution of the C-H stretch for Ag-DLC film containing 5.7 at % Ag.

Table 5-7 FTIR vibrational mode assignment in the C-H stretch region for Ag-DLC film containing 5.7at% Ag.

| Ag-DLC28 (5.7 at %) $sp^3/(sp^2+sp^3)$ ratio : 47.7 % | | |
|---|---|---|
| **Wavenumber, $cm^{-1}$** | **Assignment** | **Peak contribution, %** |
| 2840 | $sp^3$ $CH_2$(sym) | 12.3 |
| 2850 | $sp^3$ $CH_2$(sym) | 9.6 |
| 2890 | $sp^3$ $CH_2$(sym) | 18.1 |
| 2910 | $sp^3$ $CH_2$(sym) | 7.7 |
| 2950 | $sp^2$ $CH_2$ (sym) | 1.5 |
| 3010 | $sp^2$ CH (olefinic) | 10.7 |
| 3030 | $sp^2$ CH (olefinic) | 19.7 |
| 3080 | $sp^2$ CH (olefinic) | 9.1 |
| 3100 | $sp^2$ CH (olefinic) | 11.3 |

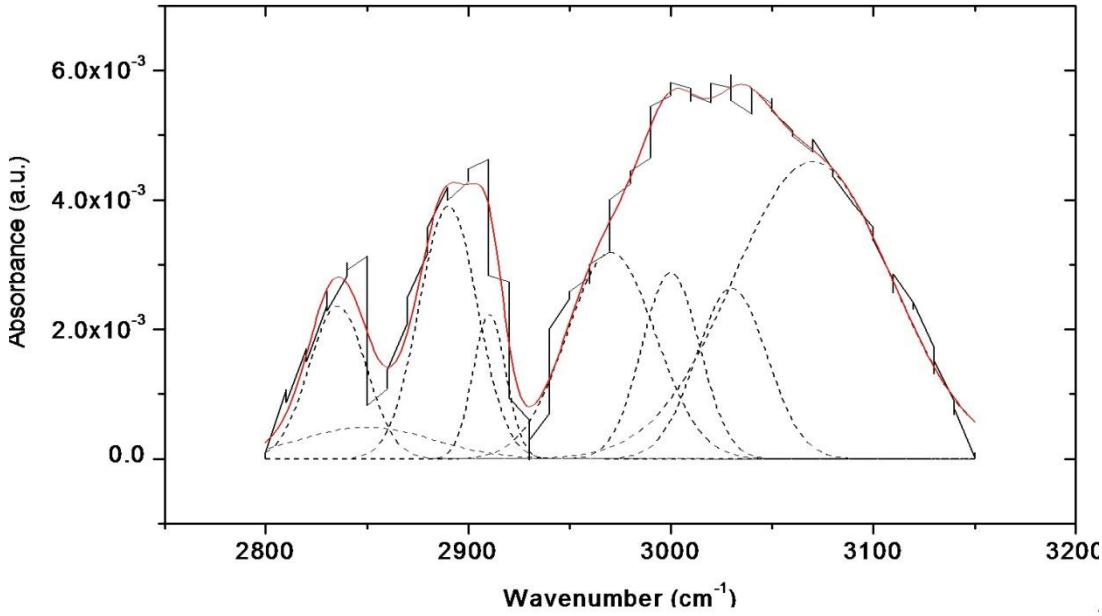


Figure 5-18 Deconvolution of the C-H stretch for Ag-DLC film containing 8.3 at % Ag.

Table 5-8 FTIR vibrational mode assignment in the C-H stretch region for Ag-DLC film containing 8.3 at% Ag.

| Ag-DLC26 (8.3 at %) $sp^3/(sp^2+sp^3)$ ratio : 42.2 % | | |
|---|---|---|
| **Wavenumber, $cm^{-1}$** | **Assignment** | **Peak contribution, %** |
| 2835 | $sp^3$ $CH_2$(sym) | 7.3 |
| 2850 | $sp^3$ $CH_2$(sym) | 3.3 |
| 2890 | $sp^3$ $CH_2$(sym) | 12.3 |
| 2910 | $sp^3$ $CH_2$(sym) | 4 |
| 2970 | $sp^3$ $CH_3$(asym) | 15.3 |
| 3000 | $sp^2$ CH (olefinic) | 9 |
| 3030 | $sp^2$ CH (olefinic) | 10.1 |
| 3070 | $sp^2$ CH (olefinic) | 38.7 |

As seen in Figure 5-19, FTIR spectra show that as the Ag content increases into DLC, the $sp^3$ content decreases. It may thus be inferred that the DLC films became $sp^2$ rich with increased

incorporation of silver nanocrystallites. Similar trends have been observed for other metal doped DLC films.

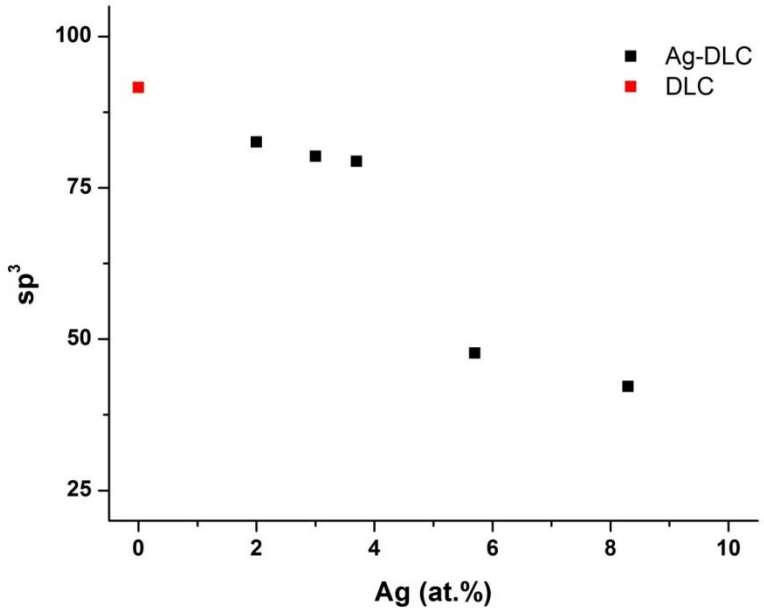


Figure 5-19 Variation of $sp^3/(sp^2+sp^3)$ ratio based on C-H bonds with Ag content in DLC films.

5.1.4 Raman Spectroscopy

Raman measurements were carried out with a laser wavelength of 532 nm. A low input power of 2.5 mW was used in order to minimize possible beam-heating effects. All bands in the Raman spectra have been fitted using a Gaussian line shape. Raman spectra can provide much information about the DLC films structure due to its ability to distinguish $sp^3$ and $sp^2$ bonding type. In general, the Raman spectra of amorphous carbon film consists of a broad peak at 1550 $cm^{-1}$, G line and a shoulder at 1350 $cm^{-1}$, D line. The G peak is a measure of the presence of $sp^2$ bonded carbon in all possible forms and contributed to the graphite. The D peak is a measure of the presence of 6-fold ring structure and contributed to the disordered

graphitic carbon. It is empirically known that the G-peak position of Raman spectra shifts to a higher wave number as the graphite component in the film increases.

Figure 5-20 indicates a series of Raman spectra of DLC and Ag doped DLC of various Ag content. As seen in Figure 5-20, the D peaks and G peaks are in the range of 1377-1381 $cm^{-1}$ and 1540-1590 $cm^{-1}$, respectively. With increasing Ag content into DLC, the peak located at around 1380 $cm^{-1}$(D-line) appears and the intensity and width of it increases. The peak positions of the G-lines varied between 1540 and 1590 $cm^{-1}$ for films deposited with different Ag content. This may be due to the variation of microstructure of the films and associated quality of graphitic carbon in the films. The intensity of the D-line was seen to increase with the increasing metal content in the DLC matrix. This would mean that metal inclusion would favor the formation of $sp^2$ bonded carbon [64]. Thus, the Raman studies indicated that these films were composed of $sp^2$ bonded carbon atoms dispersed in a $sp^3$ bonded carbon matrix.

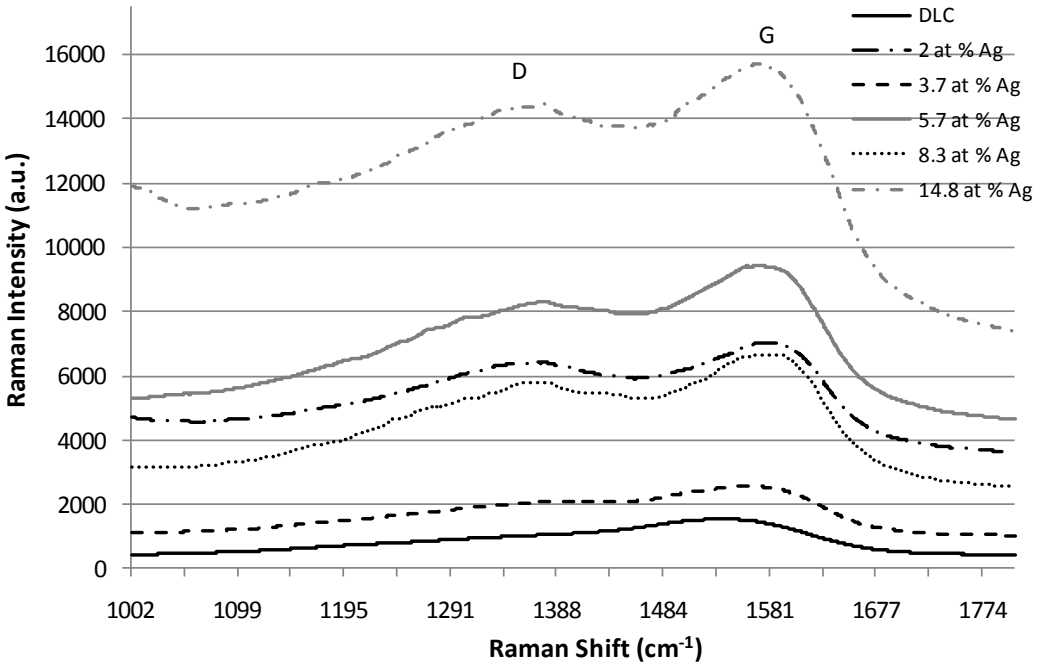


Figure 5-20 Raman spectra of DLC and Ag doped DLC of various Ag content.

Figure 5-21 and Figure 5-22 show the variation of the Raman G-peak and D-peak shift and the FWHM (full width at half maximum) and $I_D/I_G$ (the ratio of intensity of the D band to that of the G band) ratio of DLC and Ag-DLC films as a function of Ag content, respectively. These curves were derived from the Raman spectra in Figure 5-20. As seen in Figure 5-21, Ag content into DLC shifted the G peak toward higher wave number when compared to pure DLC. There is no linear relationship between increasing Ag and G peak shifting. After shifting higher wave number up to 2 at % Ag, the G peak moved lower wave number for 3.7 at % Ag. After that point, the G peak shifted higher wave number again up to 8.3 at % Ag, and then it moved lower wave number for 14.8 at % Ag. However, in this study, the D peak position did not indicate any significant change with increasing Ag content for DLC and Ag doped DLC thin films.

The $I_D/I_G$ ratio of silver containing DLC could be seen to increase when compared to pure DLC. But, the FWHM of G-peak decreased for Ag doped DLC thin films. However, as

similar like G peak shifting, there is no linear relationship between with increasing Ag content and $I_D/I_G$ ratio and FWHM lines. Baba et al. [57] produced Ag doped DLC films by magnetron plasma source ion implantation and observed that the $I_D/I_G$ ratio increased and FWHM of G-peak decreased with Ag introducing into DLC. In Raman spectra, shifting the G band to a higher wavenumber; increasing the ratio of $I_D/I_G$, and reducing the FWHM of the G band demonstrate that contribution of metal in the DLC film increases the content of $sp^2$ carbon. The results of Raman analysis is in conformity with findings from FTIR studies.

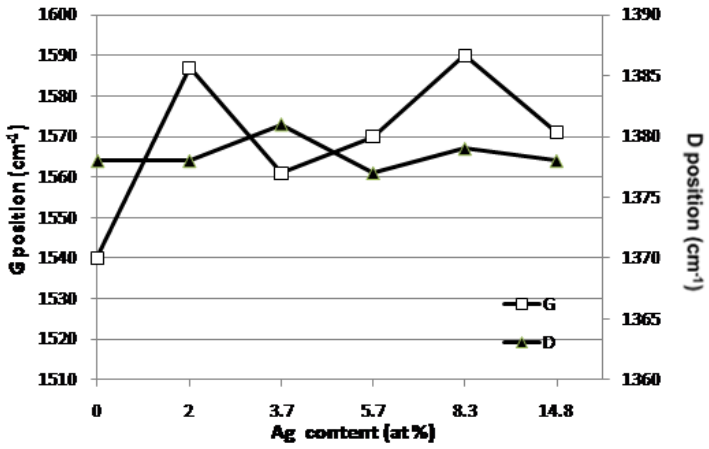


Figure 5-21 Variation of G-peak and D-peak positions of Raman spectra as a function of Ag content for DLC and Ag-DLC thin films.

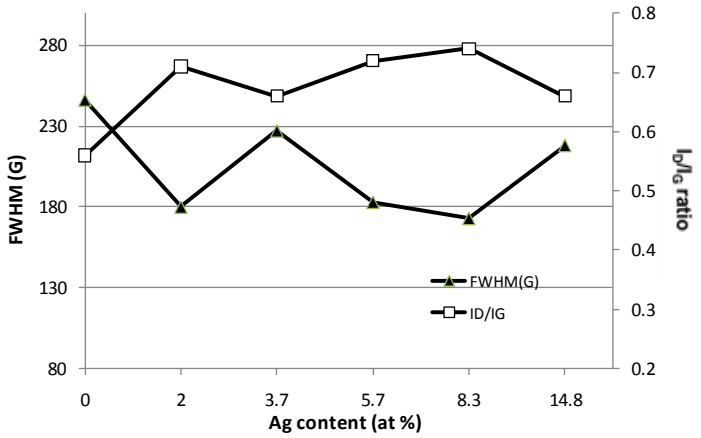


Figure 5-22 Variation of FWHM of G-peak and $I_D/I_G$ ratio of Raman spectra as a function of Ag content for DLC and Ag-DLC thin films.

## 5.2 Tribological and Mechanical testing

### 5.2.1 Nanoindentation

Nanohardness results of the DLC and Ag-DLC films are shown in the Figure 5-10. It is seen that with increase in Ag content in DLC films, the hardness values increased. It is contradictory when compare with the previous research. Because, the $sp^3$ content decreases with increase in metal content resulting in lower hardness. This trend has been observed in other Me-DLC [24, 37]. In Me-DLC, the C-C network is broken down by the presence of metal nanoparticles and this results decrease in hardness.

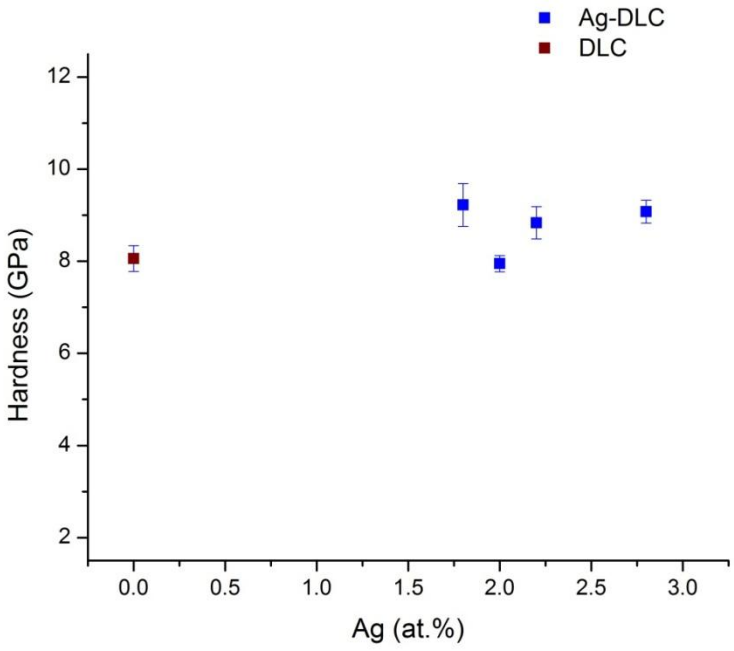


Figure 5-23 Hardness of DLC and Ag-DLC films.

5.2.2 Pin-on-disc

Pin-on-disc experiments were performed on both DLC and Ag-DLC samples with different Ag content. Since the thickness of Ag-DLC films was lower, the test was run for 1000 m for both DLC and Ag-DLC films respectively. It was observed that the friction coefficient decreases with time in DLC film as shown in Figure 5-24. This is mainly due to wear induced graphitization occurring at the contact point and is in accordance with the model proposed by Liu and Meletis [8]. But, for Ag-DLC samples, coefficient of friction is increased with time due to increase of Ag content in DLC matrix or the enrichment of the transfer layer with Ag nanoparticles.

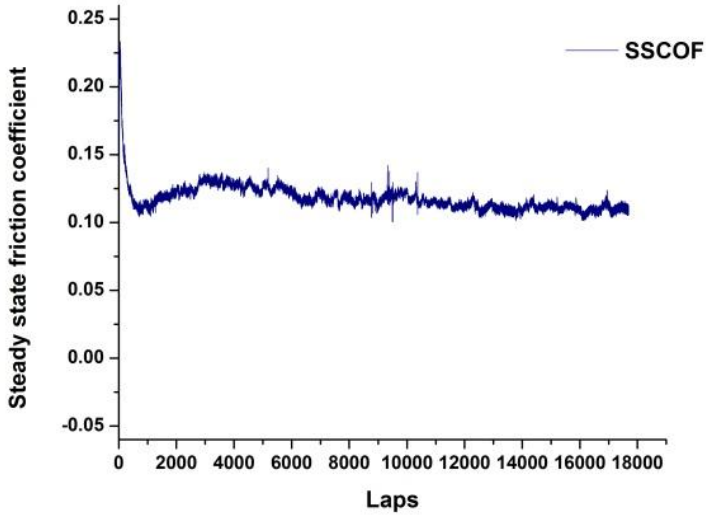


(a)

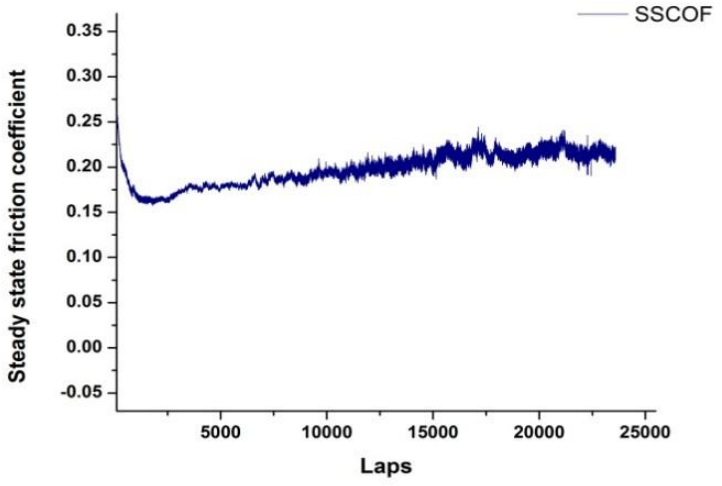


(b)

Figure 5-24 Steady state coefficient of a) DLC and b) Ag-DLC films (2.8 at.% Ag).

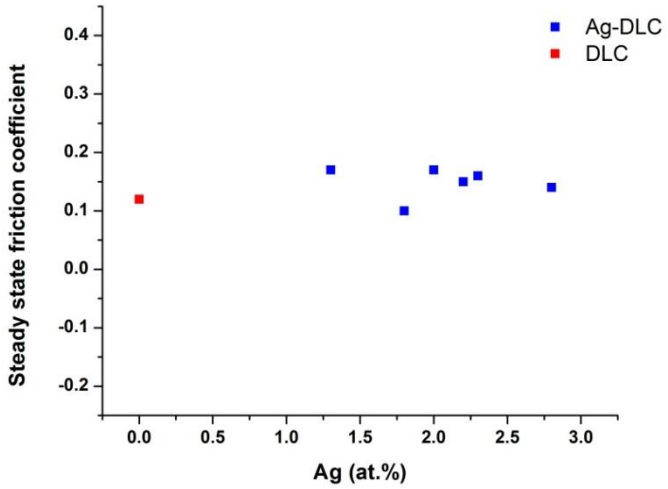


Figure 5-25 Friction coefficient of DLC and Ag-DLC films.

The wear tracks obtained after the experiment were measured by stylus profilometer for wear rate measurement. The morphology of the wear tracks DLC and Ag-DLC films were measured by stylus profilometer and the wear rates were calculated. The DLC wear track shows low depth suggesting a short range material removal. This is due to hard DLC film showing minimum wear. But in Ag-DLC films have higher depth wear track, suggesting more removal with the increase in Ag doping. It was also observed that the wear rate is increased gradually with increase in Ag content compared with DLC films. However, the wear rate remained at low levels having values up to $1.7 \times 10^{-7}$ $mm^3/Nm$ for the film with 3 at.% Ag.

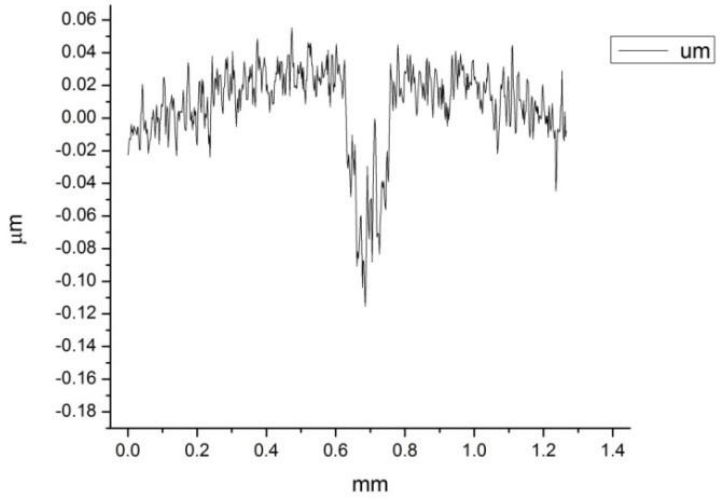


(a)

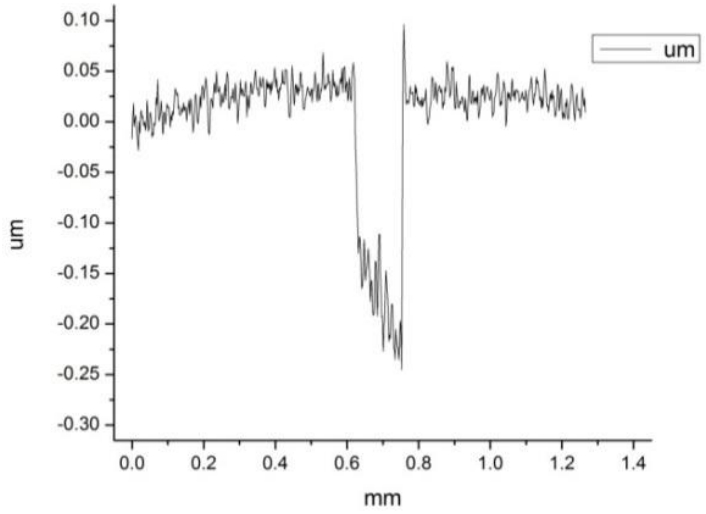


(b)

Figure 5-26 Wear track morphology of a) DLC film and b) Ag-DLC film (2.8 at.% Ag).

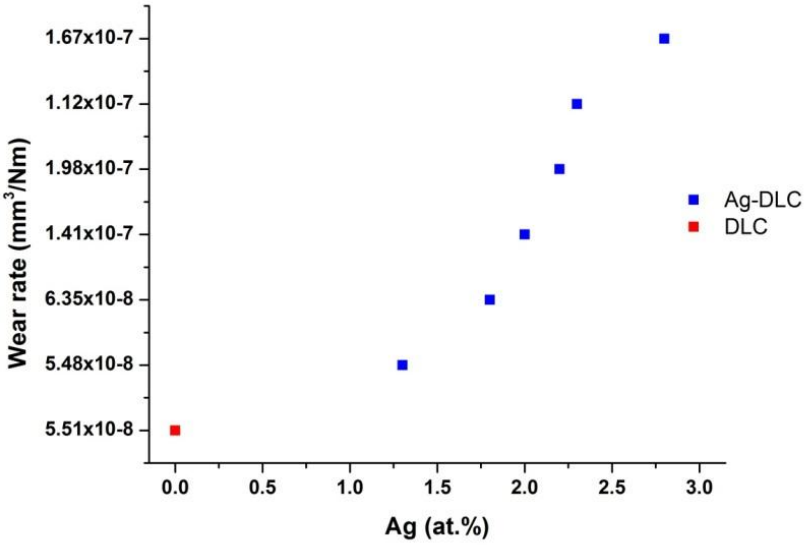


Figure 5-27 Wear rate of DLC and Ag-DLC films.

# CHAPTER 6

# CONCLUSIONS

1. This work shows the possibility of depositing good Ag doped DLC films without any considerable degradation of the hardness, friction and wear rate when compared with DLC films.
2. There is significant influence from process parameters, so they could be controlled in order to improve the quality of the film and also to increase the Ag content in the DLC matrix.
3. TEM observations revealed that the films contain a uniform distribution of Ag nanoparticles in an amorphous DLC matrix but also revealed that Ag content is decreasing with time in the direction of film growth due to poisoning of the target.
4. XPS, FTIR and Raman analysis showed that the $sp^2$ content of the films increased by increasing Ag content resulting in a subsequent reduction in hardness.
5. Based on the present results, functionality of Ag-DLC can be achieved by deposition of a top Ag-DLC layer on a pure DLC under layer.

REFERENCES

1. J. Robertson, Properties of Diamond like carbon, Surface and Coating Technology, 50 (1992) 185.

2. A.A. Voevodin, J.P. O'Neill, J.S. Zabinski, Nanocomposite Tribological Coatings for Aerospace Applications, Surface and Coating Technology., 116 (1999) 36.

3. J.S. Wang, Y. Sugimura, A.G. Evans, W.K. Tredway, The mechanical performance of DLC films on steel substrates, Thin Solid Films, 325 (1998) 163.

4. A. Grill, Review of the tribology of diamond-like carbon, Wear 168 (1993) 143.

5. K.H. Habig, Fundamentals of the tribological behaviour of diamond, diamond- like carbon and cubic boron nitride coatings, Surface and Coating Technology, 76 (1995) 540.

6. A. Erdemir, C. Bindal, J. Pagan, P. Wilbur, Characterization of transfer layers on steel surfaces sliding against diamond-like hydrocarbon films in dry nitrogen, Surface and Coating Technology, 76 (1995) 559.

7. Z.L. Akkerman, H. Efstathiadis, F.W. Smith, Thermal stability of diamond-like carbon films, Journal of Applied Physics, 80 (1996) 3068.

8. Y. Liu, E.I. Meletis, Evidence of graphitization of diamond-like carbon films during sliding wear. Journal of Materials Science, 32 (1997) 3491.

9. D. Sheeja, B.K. Tay, K.W. Leong, C.H. Lee, Effects of thermal annealing on amorphous carbon nitride films by r.f. PECVD, Diamond and Related Materials, 11 (2002) 1643.

10. Y. Pauleau, F. Thiery, Deposition and characterization of nanostructured metalycarbon composite films, Surface and Coatings Technology, 180 (2004) 313.

11. Sk. Faruque Ahmed, Myoung-Woon Moon, Kwang-Ryeol Lee, Effect of silver doping on optical property of diamond like carbon films, Thin Solid Films 517 (2009) 4035.

12. S.C.H. Kwok, W. Zhang, G.J. Wan, D.R. McKenzie, M.M.M. Bilek, Paul K. Chu,

Hemocompatibility and anti-bacterial properties of silver doped diamond-like carbon prepared by pulsed filtered cathodic vacuum arc deposition, Diamond and Related Materials 16 (2007) 1353.

13. F.R. Marciano, L.F. Bonetti, R.S. Pessoa, J.S. Marcuzzo, M. Massi, L.V. Santos, V.J. Trava-Airoldi, The improvement of DLC film lifetime using silver nanoparticles for use on space devices, Diamond and Related Materials 17 (2008) 1674.
14. Sk. Faruque Ahmed, Myoung-Woon Moon, and Kwang-Ryeol Lee, Enhancement of electron field emission property with silver incorporation into diamondlike carbon matrix, Applied Physics Letters, 92 (2008) 193502.
15. H.L. Lee, J.M. Ting, Carbon-based composite thin films for use as microelectrode, Materials Chemistry and Physics, 82 (2003) 567.
16. A. Grigonis, Z. Rutkuniene, V. Kopustinskas, G.J. Babonas, A. Reza, Investigation of optical properties of a-C:H films deposited from acetylene using direct ion beam deposition method, Vacuum, 78 (2005) 593.
17. L. Holland, S.M. Ojha, The growth of carbon films with random atomic structure ion impact damage in a hydrocarbon plasma, Thin Solid Films, 58 (1979) 107.
18. M. Weiler, S. Sattel, K. Jung, H. Ehrhardt, V. Veerasamy, J. Robertson, Highly tetrahedral, diamond- like amorphous hydrogenated carbon prepared from a plasma beam source, Applied Physics Letters, 64 (1994) 2797.
19. J. Robertson, Diamond like amorphous carbon, Materials Science and Engineering R, 37 (2002) 129.
20. K. Yamamoto, K. Wazumi, T. Watanabe, Y. Koga, S. Iijima, Tribological properties of diamond-like carbon films prepared by mass-separated ion beam deposition, Diamond and Related Materials, 11 (2002) 1130.
21. D. Sheeja, B.K Tay, S.P Lau, X Shi, X Ding, Structure and tribological characterization of

multilayer ta-C films prepared by filtered cathodic vacuum arc with substrate pulse biasing, Surface and Coating Technology, 132 (2000) 228.

22. S. Swann, Magnetron sputtering, Physics Technology, 19 (1988) 67.

23. G. Dearnaley, J. H. Arps, Biomedical applications of diamond-like carbon (DLC) coatings: A review, Surface and Coating Technology, 200 (2005) 2518.

24. C. Corbella, M.Vives, A. Pinyol, E. Bertan, C. Canal, M. C. Polo, J. L. Andujar, Preparation of Metal (W, Mo, Nb, Ti) containing a-C:H films by reactive magnetron sputtering, Surface and Coating Technology, 409 (2004) 1777.

25. P. Gupta, V. Singh, E.I. Meletis, Tribological behavior of plasma-enhanced CVD a-C:H films. Part I: effect of processing parameters, Tribology International, 37 (2004) 1019.

26. P. Gupta, E. I. Meletis, Tribological behavior of plasma-enhanced CVD a-C:H films. Part II: multilayers, Tribology International, 37 (2004) 1031.

27. J. Robertson, Mechanism of $sp^3$ bond formation in the growth of diamond-like carbon, Diamond and Related Materials, 14 (2005) 942.

28. J. Robertson, Electronic structure of diamond-like carbon, Diamond and Related Materials, 6 (1997) 212.

29. H. X. Li, T. Xu, J. M. Chen, H. D. Zhou, H.W. Liu, The effect of applied dc bias voltage on the properties of a-C:H films prepared in a dual dc-rf plasma system, Applied Surface Science, 227 (2004) 364.

30. J. Robertson, Deposition mechanisms for promoting $sp^3$ bonding in diamond-like carbon, Diamond and Related Materials, 2 (1993) 984.

31. C. Casiraghi, A.C. Ferrari, Raman spectroscopy of hydrogenated amorphous carbons, J. Robertson, Physical Review B, 72 (2005) 085401.

32. J. Robertson, Ultrathin carbon coatings for magnetic storage technology, Thin Solid Films, 383 (2001) 81.

33. A. Erdemir, C. Donnet, Tribology of diamond-like carbon films: recent progress and future prospects, Journal of Applied Physics, 39 (2006) 311.
34. C. P Klages and R. Memming, Microstructure and Physical properties of Metal-containing hydrogenated carbon films, Material Science Forum, 52 (1989) 609.
35. Y. Chang, D. Y. Wang, W. Wu, Catalysis effect of metal doping on wear properties of diamond like carbon films deposited by a cathodic arc activated deposition process, Thin Solid Films, 420 (2002) 241.
36. S. Gunjan, Fabrication and characterization of cobalt-diamond-like carbon nanocomposites, The University of Texas at Arlington, 2007.
37. V. Singh, J. C. Jiang, E.I. Meletis, Cr-Diamondlike carbon nanocomposite films: Synthesis, Characterization and properties, Thin Solid Films, 489 (2005) 150.
38. N. Ali, Y. Kousar, T. L. Okpalugo, V. Singh, M. Pease, A. A. Ogwu, J. Gracio, E.I. Meletis, M.J. Jackson, Human micro-vascular endothelial cell seeding on Cr-DLC thin films for mechanical heart valve applications, Thin Solid Films, 515 (2006) 59.
39. R.J. Narayan, H. Wang, A. Tiwari, Nanostructured DLC-Ag composites for biomedical applications, Material Research Society Symposium Proceedings, 750 (2003) 205.
40. C. P. Lungu, Nanostructure influence on DLC-Ag tribological coating, Surface and Coating Technology, 200 (2005) 198.
41. H.S. Zhang, J.L. Endrino, A. Anders, Comparative surface and nano-tribological characteristics of nanocomposite diamond-like carbon thin films doped by silver, Applied Surface Science 255 (2008) 2551.
42. C.P. Lungu, I. Mustata, G. Musa, V. Zaroschi, A. M. Lungu, K. Iwasaki, Low friction silver DLC coatings prepared by thermionic vacuum arc method, Vacuum 76 (2004) 127.
43. R. J. Narayan, Pulsed laser deposition of functionally gradient diamond-like carbon–metal nanocomposites, Diamond and Related Materials 14 (2005) 1319.
44. X. Yu, M. Hua, C. Wang, Influence of Ag content and nano grain size on microstructure,

mechanical and sliding tribological behaviors of Ag-DLC films, Journal of nanoscience and nanotechnology, 9 (2009) 6366.

45. P. Hazarika, Synthesis, structure and characterization of Ag doped DLC thin films, The University of Texas at Arlington, 2007.
46. T. A. Friedmann, K. F. McCarty, J. C. Barbour, M.P BartSiegal. D. C. Dibble, Thermal stability of amorphous carbon films grown by pulsed laser deposition, Applied Physics Letters, 68 (1996) 1643.
47. D. Nir., Intrinsic stress in diamond-like carbon films and its dependence on deposition parameters, Thin Solid Films 146 (1987) 27.
48. M. Weiler, S. Sattel, T. Giessen, K. Ehrhardt, Preparation and properties of highly tetrahedral hydrogenated amorphous carbon, Physics Review B, 53 (1996) 1594.
49. J.P. Sullivan, T.A. Friedmann, A.G. Baca, Stress relaxation and thermal evolution of film properties in amorphous carbon, Journal of Electronic Materials, 26 (1997) 102
50. P. Koidl, C. Wild, B. Dischler, J. Wagner, M. Ramsteiner, Properties and characterization of amorphous carbon films, Materials Science Forum, 52 (1989) 41.
51. M. Crischke, K. Bewilogua, K. Trojan. Dimigen, Application-oriented modifications of deposition processes for diamond-like-carbon-based coatings, Surface and Coatings Technology, 74 (1995) 739.
52. M.D. Bentzon, K. Mogensen, J.B. Hansen, C. Barholm-Hansen, C. Taholt, P. Holiday, S.S. Eskildsen, Metallic interlayers between steel and diamond-like carbon, Surface and Coatings Technology, 68 (1994) 651.
53. J Narayan, RD Vispute, K Jagannadham, interfacial processing and adhesion of diamond, diamond-like, and tin films on metallic and polymeric substrates, Adhesion Journal of Science and Technology, 9 (1995) 753.

54. K. Yamamoto, K. Wazumi, T. Watanabe, Y. Koga, S. Iijima, Characteristics of nickel-containing carbon films deposited using electron cyclotron resonance CVD, Diamond and Related Materials, 11 (2002) 1131.
55. L. Xia, G. Li, The frictional behavior of DLC films against bearing steel balls and $Si_3N_4$ balls in different humid air and vacuum environments, wear 264 (2008) 1077.
56. H. Dimigen, C.P. Klages, Microstructure and wear behavior of metal-containing diamond-like coatings, Surface and Coatings Technology, 49 (1991) 543.
57. K. Baba, R. Hatada, S. Flege, W. Ensinger, Preparation and Properties of Ag-Containing Diamond-Like Carbon Films by Magnetron Plasma Source Ion Implantation, advances in material science and engineering, 2012 (2012).
58. Q. Wei, A.K. Sharma, J. Sankar, J. Narayan, Mechanical Properties of diamond like carbon composite thin films prepared by pulsed laser deposition, Composites part B: Engineering, 30 (1999) 675.
59. NASA, Better bone implants, 2002. Retrieved from http://science.nasa.gov/science-news/science-at-nasa/2002/30oct_hipscience/
60. Casiraghia, A.C. Ferrari, R. Ohr, D. Chu, J. Robertson, Surface properties of ultra-thin tetrahedral amorphous carbon films for magnetic storage technology, Diamond and Related Materials, 13 (2004) 1416.
61. D.R. McKenzie, S.C.H. Kwok, M.M. Bilek, D.G. McCulloch, P.K. Chu, Soft ferromagnetic materials based on iron/carbon multilayers, Physica B, 394 (2007) 273.
62. N. Gopinathan, C. Robinson, F. Ryan, Characterization and properties of diamond-like carbon films for magnetic recording application, Thin Solid Films, 355 (1999) 401.
63. K.M. Krishna, M. Umeno, Y. Nukaya, T. Soga, T. Jimbo, Photovoltaic and spectral photoresponse characteristics of n-C/p-C solar cell on a p-silicon substrate, Applied Physics Letters, 77 (2000) 1472.

64. S.J. Bull, Tribology of carbon coatings: DLC, diamond and beyond, Diamond and Related Materials 4 (1995) 827.

## BIOGRAPHICAL INFORMATION

Venkatesh Majji was born in March 1990, in Srikakulam, India. He received his bachelor degree in Metallurgical Engineering from Jawaharlal Nehru Technological University, Hyderabad, India in 2011. His undergraduate research work was involved in the field of Nanomaterials and Tribology. He has written his bachelor's thesis on flow behavior of cu-4ti-1cr alloy. After completing his undergrad studies, his aim was to pursue masters. Then went to University of Texas at Arlington and started his Masters in August 2011. While he was a graduate student, his research work mainly focused on thin film coatings in the Surface and Nano-engineering laboratory. These research projects involve more about CVD and PVD systems processing and growing thin films, which have numerous applications in automobiles, optical devices, biomedical implants and etc. He is a candidate for the degree of Master of Science in Materials Science and Engineering to be awarded in May 2013.